ABSTRACT

Lycophyte *Huperzia lucidula* Morphological, Physiological, and Modeling Response to Paleozoic Environmental Conditions

Christopher J. A. Skrodzki, M.S.

Mentor: Joseph D. White, Ph.D.

An extant lycophyte, *Huperzia lucidula*, was studied to determine its response to higher atmospheric pressure and oxygen. This study answers two central questions: Do extant lycopsids respond to the atmospheric conditions of their ancestors? Is lycopsid gas exchange accurately modeled using current methods? By provides protocols for growing plants under the effect of various atmospheric conditions, this work demonstrates that atmospheric pressure is capable of effecting plants without changing the concentration of substrate active atmospheric gases and determines the effect of changed oxygen concentration on previously developed plants. Previous works have focused on the combined effect of pressure with increased CO_2 or on pressurizing plant products. This work furthers understanding of how ecosystem properties, such as canopy carbon assimilation, are likely heavily regulated by subsurface morphology. This research in terrestrial and synthetic atmospheres also suggests methods for growing plants more efficiently in water and light limited environments, potentially deep-space.

Lycophyte *Huperzia lucidula* Morphological, Physiological, and Modeled Response to Paleozoic Environmental Conditions

by

Christopher J. A. Skrodzki, B.S.

A Thesis

Approved by the Department of Biology

_____

Dwayne D. Simmons, Ph.D., Chairperson

Submitted to the Graduate Faculty of
Baylor University in Partial Fulfillment of the
Requirements for the Degree
of

Master of Science

Approved by the Thesis Committee

_____

Joseph D. White, Ph.D., Chairperson

_____

Sanghoon Kang, Ph.D.

_____

Daniel Peppe, Ph.D.

Accepted by the Graduate School

May 2017

_____

J. Larry Lyon, Ph.D., Dean

Page bearing signatures is kept on file in the Graduate School.

TABLE OF CONTENTS

LIST OF FIGURES

LIST OF TABLES

LIST OF ABBREVIATIONS

a_{max} – maximal stomatal aperture area

a_{max} – mean stomatal aperture area

ELISA – Enzyme-Linked ImmunoSorbent Assay

ETR – linear Electron Transport Rate

g_{CO_2} – carbon dioxide gas conductance

g_{H_2O} – water vapor conductance

g_b – boundary layer conductance

g_l – leaf conductance

g_m – mesophyll conductance

g_{min} – minimum g_{cut} velocity

g_s – stomatal conductance

IRGA - InfraRed Gas Analysis

LPP - Lycopsid Photosynthetic Pathway

PAR – Photosynthetically Active Radiation

PLUE – PAR Light Use Efficiency

ΦPSII – PhotoSystem II Quantum Yield

MSL – Mean Sea Level

RuBisCO – Ribulose-1,5-Bisphosphate Carboxylase/Oxygenase

SEM – Scanning Electron Microscopy

SI – Stomatal Index

SLA – Specific Leaf Area

SPAC – Soil Plant Atmosphere Continuum

SSC – SubStomatal Cavity

TEM – Transmission Electron Microscopy

VPD – Vapor Pressure Deficit

WUE – (instantaneous) Water Use Efficiency

WUEi – intrinsic Water Use Efficiency

ACKNOWLEDGMENTS

I would like to first and foremost sincerely thank Dr. White for helping me maintain a clear sense of focus for this thesis work, his honest critique and assistance editing this work, and for inexorable patience in assisting me through this entire process.

This material is based upon work supported by the National Science Foundation under Grant No. 1338247.

I would also like to thank Dr. Bernd Zechmann (Center for Microscopy and Imaging, Baylor University) for scanning electron microscopy and sample preparation technical support.

Additionally, I cordially thank Tamura Dunbar, Cameron Miller, Jake Arterbury, and Matthew Moreno for experimental support.

To all hardworking diaspora

Although you sacrifice the connections to your families, your wealth, and your comfort, you produce the greatest people of each generation- a person is only as good as by the perspectives that which they have to draw upon.

~Thank you and maintain your fortitude.

CHAPTER ONE

Introduction

Lycophytes, also known as lycopsids, are one of the most basal extant lineages of all vascular, non-seeding, plants and are considered polyphyletic to those of modern tracheophytes (Bateman, 1990). Lycopsid plants are thought to have derived from leafless zosterphylls or possibly also leafless G-type tracheid *Asterxylon sp.* plants (Crane et al., 2004; Kenrick and Crane, 1997). The earliest lycophyte *Baragwanathia longifolia* fossils have been placed between 420-410 Mya, possibly encompassing the late Silurian (Lang and Cookson, 1935; Rickards, 2000). However, lycopsids are perhaps best known for the first non-fern ally/microphyllus arborescent *Sigillaria sp.* and *Lepidodendron sp.* of the Sigillarianae Superfamily (Beck, 1962; DiMichele and Bateman, 1996). L*epidodendron sp.* maintained canopy dominance during the middle Carboniferous and its fossils have been placed at 370Mya, well into the early Devonian (Dimichele et al., 2009; Meyer-Berthaud and Decombeix, 2007; Willis and McElwain, 2002).

Arborescent Lycopsids

Arborescent lycopsid, *Lepidodendron sp.,* dominated habitats that were transitionary in nature (Dimichele and Phillips, 1988). These coal swamps are the source of the dubiously forming coal-ball deposits. While it is disputed as to whether these formed due to the influx of salt or freshwater, it seems unanimous that coal swamps were characterized by flooding (Raymond et al., 2010; Scott et al., 1996). This flooding greatly

limited the diversity of these swamps, as few plants were capable of thriving within these peat concentrated and nutrient limited environments (Dimichele and Phillips, 1985).

Various strategies have been suggested in order to allow lycopsids to flourish within these unstable environments. This habitat suggests that coal swamp lycopsids had ecologically determined life-cycles, where lycopsids would spend a relatively large period of time within a vegetative phase followed by a relatively short crowning and cone-bearing stage. Complex genus specific rhizome organizations also differentiated arborescent lycopsids from one another (DiMichele and Bateman, 1996); while providing anchoring that must have been necessary to grow on unstable peat yet still grow up to 40 m, this is evidenced in how roughly 25% of all recovered lycopsid biomass was root material (Dimichele and Phillips, 1985). In order to prevent intraorder (Isoetales) competition, it has been proposed that the time of the reproductive stage, cone location, crown height, and cone architecture was varied between lycopsid species, yet all scale trees were heterosporous and of determinate growth (Dimichele and Phillips, 1985). Regardless of the unique features between arborescent lycopsid species, the presence of many leaf scars on tree bark is the most conspicuous feature that defines scale trees and is shared between all of these species; these leaf scars are caused by the leaves that connected directly to the vascular system through a ‘parichnos tissue’ (DiMichele and Bateman, 1996; Dimichele and Phillips, 1985). Fossil evidence has substantiated from the presence of leaf scars that leaves coated these trees from trunk to crown (Wang et al., 2002). Clearly, this suggests that a key trait that allowed lycopsid dominance lied within the large presence of microphyllus leaf material, all bearing this parichnos tissue morphology.

Structure and Function of Parichnos Tissue

First described in *Lepidodendron Harcourtii*, the presence of parichnos tissue beneath leaf scars and penetrating the periderm is a defining characteristic of all arborescent lycopsids of the Sigillarianae Superfamily (Bertrand, 1891; DiMichele and Bateman, 1996). Parichnos tissue originates from the middle cortex, passes through suberized zones, and generally bifurcates in the outer cortex to the base of each leaf; additionally, parichnos tissue has been described as being lined with other delicate, non-secretory, tissues and loses bifurcation in mature leaves to define empty spaces in parenchyma tissue; additionally, this tissue has been identified within both trunk and spore-bearing crown leaves (Hill, 1906). The ubiquity of this tissue and general structure seem to suggest that this is no so much a resultant tissue as this is a general morphology. Additionally, since extant Isoetes plants do not exhibit parichnos, elucidating the function of parichnos morphology is dubious.

Despite this, recent work has made parallels between extinct parichnos tissue to that of modern aerenchyma (Green, 2014). This position is attractive as aerenchymal tissue characterizes many extant herbaceous non-aquatic lycopsids (Chu, 1974). Yet, the current function of aerenchymal tissue has been best described within both leaf and rhizome tissue of many non-lycopsid aquatic plants, forcing oxygen from leaves to roots but carbon dioxide gas from roots to water exposed leaves (Dacey, 1980). Despite the different in habit, it has been suggested to have a similar function within arborescent terrestrial lycopsids to that of aquatic angiosperms; however, arborescent lycopsids instead would draw carbon dioxide from the soil as opposed to from water submerged leaves. The crux of this reasoning is that atmospheric levels of high oxygen/low carbon

dioxide gas would be not ideal for leaf surface gas exchange. This function of aerenchyma within lycopsids has been substantiated to define a novel metabolic system, similar to that of aquatic CAM, unique to terrestrial lycopsids, coined as the Lycopsid Photosynthetic Pathway (LPP) (Green, 2010). However, aerenchyma has been observed within the leaves and roots of various non-aquatic angiosperms (Drew et al., 2000). Additionally, this does not seem efficient, since the presence of many microphyllus leaves suggests a large plant gas exchange surface, as opposed to green stemmed *Calamites sp*. that were also present within coal swamps (Raymond et al., 2010). Regardless, the suggestion that parichnos tissue is an early morphology allowing the organization of aerenchymal tissue seems reasonable from a homologous morphology perspective (Green, 2010); and a point of consensus seems to be that the function of aerenchyma is to allow/direct the flow of gas through relatively dense plant tissues.

Aerenchyma as Pipes

Considering aerenchyma morphology as a method to improve gas inflow into plant leaves satisfies Green's reasoning for the necessity of parichnos tissue. The ability to concentrate carbon dioxide gas despite low atmospheric levels within Paleozoic coal swamps suggests there is some advantage for extant non-aquatic lycopsids to maintain this morphology. This presupposes that terrestrial plants do not obtain the majority of their carbon dioxide from soil sources.

A key point in the argument for LPP is the physiological action of carbon dioxide concentration within hydrophyte plants overnight (Constable et al., 1992). This clearly seems to indicate that a unique feature of aerenchymal tissue is to store carbon dioxide gas while photosynthetic demands are not high and not related to temperature. This is

feature is clearly beneficial for hydrophyte plants, which have a limited bacterially-produced supply of carbon dioxide gas. However, assuming this limitation for terrestrial plants is problematic since this would suggest that the presence of many leaves on the trunks of arborescent lycopsids were mainly for respiration and were limited in carbon dioxide assimilation. This raises issues with the physiologies of modern lycopsids, as previous research has shown lycopsid stomata are also insensitive to closing their stomata in response to humidity, controlled by changes in temperature, and only reacting to the plant water content (Soni et al., 2012). Thus, in a wetland environment, lycopsid plants would have trouble forming the seal necessary to concentrate carbon dioxide in their tissues for use during the day. Yet, in a highly disturbed environment that experiences significant drying periods, this could act as a back-up breather for arborescent lycopsids.

Another role of aerenchyma could line in its role as mesophyll tissue. Mesophyll tissue has recently been implicated in reducing the productivity of terrestrial plants (Niinemets et al., 2009). Considering that aerenchyma tissue are essentially air spaces that allow atmospheric gases to freely flow between the stomatal aperture to inner mesophyll tissues, the development of parichnos/aerenchyma tissue would clearly be an advantage to supplying air to inner mesophyll tissues within land plants. This is consistent with the presence of spongy mesophyll in relatively highly productive angiosperms.

Mechanistically, this would increase the carbon dioxide flux rate of mesophyll tissues by increasing the surface area that carbon dioxide gas phase particles are in contact with the atmosphere. These have been classically formulated as internal air-space conductance g_{ias} (Nobel, 2009). Assuming the only source of carbon dioxide gas is the

atmosphere, the contrapositive of this states that if there was a limit on atmospheric gas mesophyll flux, then there would be no aerenchyma tissue. Conceivably, if there is no aerenchyma tissue but still a limit on mesophyll flux, then it would be expected that mesophyll conductance would be lower due to thickened parenchyma cell walls, and this has not been previously observed in any lycopsids.

Currently Known Functions of Mesophyll

These changes would have significantly effects upon plant leaf function, as the mesophyll is the cell layer responsible for containing chloroplasts for photosynthesis, chlorenchyma. This is complicated by when the definition between mesophyll and epidermal cells is unclear. For example, there exist cells in-between photosynthetic and non-photosynthetic mesophyll cells known as translucent cells, generally used to define Kranz anatomy bundle-sheath cells in C4 plants (Metcalfe and Wilkerson, 1979). The interface between photosynthetic and non-photosynthetic cells is what defines the supply of carbon-fixed sugar to plant conductive tissues. Therefore, it is very reasonable to define a novel metabolic system such as LPP based only on morphologic differences from ‘standard’ C3 metabolisms.

In order to better understand what defining LPP could mean in terms of physiological carbon-fixation, it is best to understand what mesophyll features currently define C3, C4, and CAM plants. Generally, C3 is conducted within all chlorenchymal cells when adequate light and carbon dioxide is present. However, C4 tends to occur in plants exhibiting a compartmentalization of highly organized mesophyll chlorenchymal cells with little starch around poorly organized chlorenchymal bundle sheath cells with large starch granules- this is known as Kranz anatomy. CAM plants tend to have tightly

packed mesophyll and lower pH vacuoles that store malic acid diurnally (Taiz and Zeiger, 2010). LPP is a combination of C4 and CAM in this sense, whereby a unique mesophyll spatial morphology allows a temporal morphology of higher carbon dioxide storage.

CHAPTER TWO

Literature Review

Model Selection

For this study, the clubmoss species *Huperzia lucidula* was used over Isolates, Selagineles, and other Lycopodiales plants as these inhabit laboratory-prohibitively semi-aquatic habitats, have a smaller geographic distribution, are currently of endangered status, and/or possess more angiosperm-like leaf morphologies (USDA, 2015). The morphology of *H. lucidula* presents many features that simulate the physiological profiles of its extinct evolutionary ancestors in relation to the Soil Plant Atmosphere Continuum (SPAC). Additionally, extant paleo-plant models inform the probable subsurface morphology of extinct plants, allowing more accurate gas conductance modeling, rather than just the surface characteristics available through fossil study.

The phylogeny of *H. lucidula* has been established through cytotaxonomical and morphological data closely relating the species *Lycopodium lucidulum* and *Lycopodium selago* (Löve and Löve, 1958; Chu, 1974). Molecular studies have since upheld systematic division by of the order/family of Lycopidiales/Lycopodiacae, from Isoetales/Isoetaceae and Selaginales/Selaginellaceae (diverging 375-351 Mya), and into three genus: *Lycopodium*; *Huperzia*, which diverged from Lycopodium 267 Mya; and *Lycopodiella*, diverging 208 Mya from Lycopodium (Wikström and Kenrick, 2001; Yatsentyuk et al., 2001). This firmly places *H. lucidula*, or shining clubmoss, with morphology representative of its order/family from between the middle-Devonian to the

early-Carboniferous. While the genera *Selaginella* (spike moss), *Lycopodium* (club moss), and *Isoetes* (quillmoss) are representative of a pre-transitional early-late phase of the Pennsylvanian epoch (Dimichele et al., 2009) (Figure 2.1).

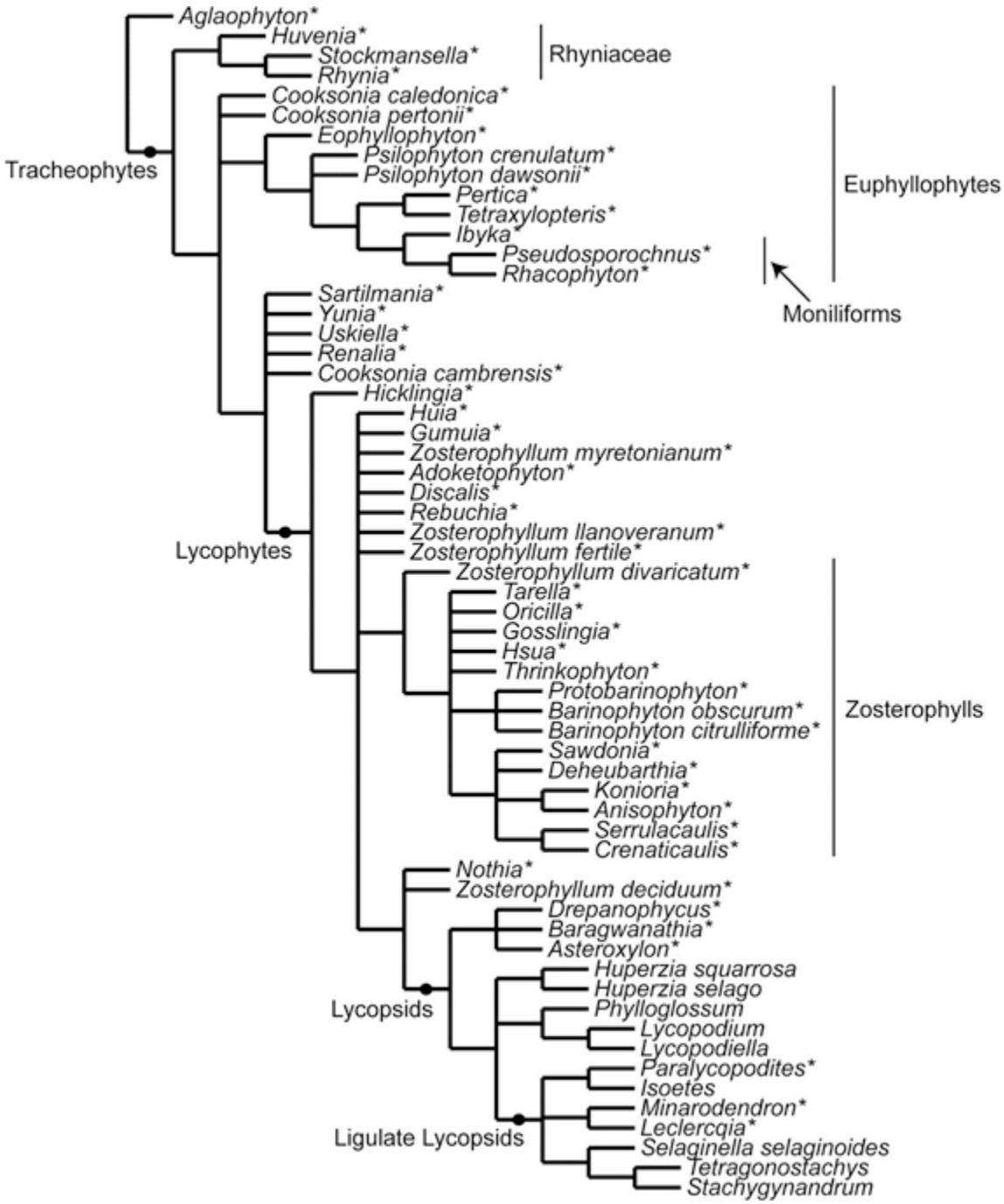

Figure 2.1 – Cladogram displaying the general phylogeny of major lycopsids groups relative to basal tracheophytes and origin zosterphylls (Crane et al., 2004).

H. lucidula allows the study of the morphological and/or physiological characteristics which may have significantly contributed to arborescent lycopsid plants maintaining a presence within the canopy following a major middle-late Pennsylvanian climatic transition. Considering a uniform atmospheric volume, higher levels of Carboniferous oxygen result in a higher atmospheric partial pressures. Current models of gas exchange indicated that changes in the partial pressure of different gas-species directly relates to changes in specie assimilation and photosynthesis (Farquhar et al., 1980). Yet, the precision of these models is suspect as these are based on angiosperm plant stomatal control characteristics (Haworth et al., 2011). Previous work has also demonstrate that tissue morphology of lycopsids has many features which are exaggerated in modern angiosperms (Chu, 1974), this could challenge evidence that suggests that only higher levels of atmospheric carbon dioxide are capable of leading to short-term decreases stomatal apertures but long-term increases stomatal densities (Beerling et al., 2001; Dow et al., 2014; Konrad et al., 2008). Consequently this suggests that current geological atmospheric models assume that the rate of lycopsid gas exchange is consistent with that of modern angiosperms. With detailed measurements of *H. lucidula* not only can current models be appropriately corrected with experimental measurements of surface and subsurface stomatal morphology, but also inform possible alterations to current gas assimilation models.

Model Morphology

Previous work has described the ability of a plant to conduct gas exchange to be affected by the leaf profile, leaf tissue organization, and stomatal distribution, which have been suggested to be effected by stomatal orientation, and guard cell lateral profile

(Beerling et al., 2001; Chu, 1974). While the reproductive method of these plants does directly affect these plants energy budgets and phylogeny by placement of sporangia, there is scant evidence to suggest that these plants' reproductive methods directly interact with the SPAC and direct the change of other characteristics in consequence of SPAC conditions in order to ensure the plants' continued survival. However, the reliance of lycopsid sporangia for dispersion by water is a likely selective pressure for larger canopy presence directing changes in gross shoot profile.

Previous work has described the ability of a plant to conduct gas exchange is affected by the plant, leaf profile, leaf tissue organization, stomatal distribution, stomatal orientation, and guard cell lateral profile. The gross shoot profile of *H. lucidula* is also strikingly similar to the possibly late Silurian *Baragwanathia longofolia*, as well the early-late Devonian *Drepanophycus spinaeformis* and *Halleophyton zhichangense* (Li et al., 2000; Li and Edwards, 1997), as it consists of a microphyll leaf structure and body plan that was favored in the early Devonian (Figure 2.2). *H. lucidula* leaves have been characterized as having a length between 7.5mm and 9.6 mm around a mean length of 8.0mm (Chu, 1974). Amateur botanists have catalogued average stem lengths in good agreement with published mean lengths of *H. lucidula* erect green axis and one half the transition zone length, 15.24cm to 15.1±3.2cm (Rook, 2004; Reutter, 1987); the average shoot height to average leaf length ratio is approximately 19:1 within both *H. lucidula* and *H. selago*. This seems to indicate that there are few marked differences between these two species in terms of gross leaf profile (Chu, 1974).

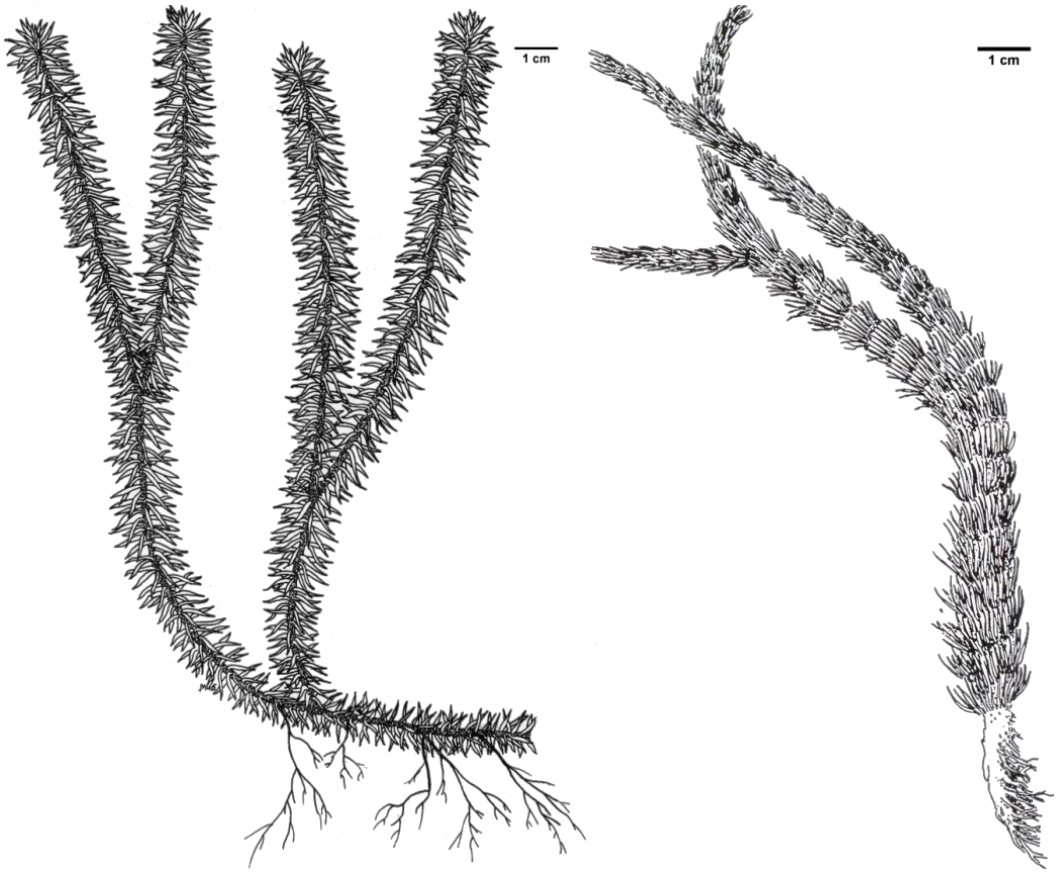

Figure 2.2 – Profile of *H. lucidula* alongside drawing of *B. longofolia* fossil (Willis and McElwain, 2002).

The mesophyll of *H. lucidula* has been described as being irregularly ovoid shaped and differentiates into neither palisade nor spongy tissue, unlike modern angiosperms. It has been suggested that unlike some extant *Huperzia* and *Lycopodium*, *H. lucidula* possesses aerenchyma, or large "air spaces," which tend to occur near the adaxial part of leaves. Yet, there are no clear published images of *H. lucidula* or special notes detailing its mesophyll distribution. This is significant in understanding the gas exchange potential of *H. lucidula* since the epidermal tissue is hypostomatal, bearing only abaxial stomata. The best published image of what the expected mesophyll distribution of *H. lucidula* is detailed in that of the closely related *L. rufescens*, which clearly exhibits a

bias in aerenchyma and possible substomatal cavities towards the abaxial region (Chu, 1974). Our research has produced clear pictures of *H. lucidula* which exhibit a similar yet unique distribution to that of *L. rufescens.*

The conductive tissue within *H. lucidula* is situated within a single small midvein composed of tracheids typically enclosed within few layers of elongated parenchyma cells structures, which notably are pitted yet lack water resistance callose material (Chu, 1974); as suggested to be representative of early vascular flora (Bierhorst, 1971; Friedman and Cook, 2000).While the stomata have been described as being an average 45.3μm in width perpendicularly and 53.3μm parallel to the leaf midline, and possess guard cells that are at the same level as the leaf surface with both outer and inner ledges (Chu, 1974). This suggests that adaxial leaf openings are over tightly arranged mesophyll tissue that retards gas flow to the far abaxial side of the leaf, suggesting that the gross mesophyll resistance of *H. lucidula* is not characterized by substomatal cavities but by the adaxial tissue.

Model Physiology

It has been suggested that microphyllus leaves were likely advantageous as this leaf form would minimize direct sun facing surface areas, effectively minimizing the total heating effect of the sun upon low transpiration rate leaves, helping cooling these leaves from reaching lethal temperatures (Beerling et al., 2001). Additionally, since the sink strength of all plant transpiration and lycopsid stomatal control is directly related to the relative humidity, dry air shifts the equilibria of water vapor outside leaf stomata causing leaves to dry and stomata to closure (Soni et al., 2012). The draw strength of vapor pressure deficit is essentially limited by relative humidity, the ratio of amount of water

vapor to that at the saturation point that is defined by temperature and pressure, even though the saturation point of water can increase in an atmosphere solely due to pressure. Since the atmospheric composition of water is essentially limited, the sink strength of vapor pressure deficit that drives plant transpiration is generally constant within an average temperature and not dependent upon atmospheric gas conditions. This suggests that the sink strength of plant transpiration is generally correlated with plant stomatal conductance which is constrained by stomatal control mechanisms.

The ability for a plant to resist droughts is an effect of a plant's ability to retrain water via water use efficiencies. This is generally s product of plant stomatal control and atmospheric gas source strength. While, *H. lucidula* has not been previously demonstrated to possess the ion based stomatal control mechanisms that are present within angiosperms (Brodribb and McAdam, 2011; Evert et al., 2006), a consequence of this is that these plants are able to effectively maximize stomatal aperture sizes via only guard cell water content. Given that larger stomatal aperture sizes maximize the influx of atmospheric gases and the rate that which water vapor can actively be lost to the atmosphere (Beerling et al., 2001; Roth-Nebelsick, 2007), and that low carbon assimilation rates would be conceivably due to low mesophyll gas conductance rates caused by the tightly packed mesophyll organization previously observed within lycopsids; this suggests that the water use efficiencies of lycopsids is entirely dependent upon atmospheric conditions to determine both the operational aperture size and atmospheric gas source strength. The atmospheric gas source strength for stomata is dependent upon atmospheric moral air density and temperatures (Franks and Farquhar, 2001); both of these can be changed by increases in gases such as carbon dioxide that

also contribute to radiative forcing , yet increases in non-forcing gases or increases in atmospheric pressures only increase moral gas densities (Graham et al., 1995; Vaughan and Lenton, 2012).

Therefore, the water use efficiencies of lycopsids is likely to have been higher during periods of high atmospheric carbon dioxide due to the increased stomatal gas flux via the increased moral air density and higher temperatures via solar forcing, if there was adequate water to support high rates of transpiration (Graham et al., 1995; Franks and Farquhar, 2001; Vaughan and Lenton, 2012). Consequently, the water use efficiency of lycopsids was likely to be also high during geological time periods with lower carbon dioxide levels yet increased atmospheric pressures. However, estimation of water use efficiency becomes dubious as the ratio of operational stomatal aperture size changes due to water conditions to that of maximal size (Konrad et al., 2008). Recent computer modeling implicated that water use efficiency increases are due to physically changes in response to the present of large substomatal cavities (Roth-Nebelsick, 2007); additionally, angiosperms have been found to significantly increase the relative size of mesophyll aerenchyma in response to drought conditions (Chartzoulakis et al., 1999). This suggests that the role of carbon dioxide gas availability is more important than water vapor to lycopsid plants in maintaining efficiency and a potential mechanism for the drought resistant properties of lycopsids, which allowed these plants to effectively survive sudden periods of drought within the middle-late Devonian (Arrigo et al., 2013; Gueidan et al., 2011)- whereby, the morphological lack of spongy mesophyll tissue, or potential stomatal-side aerenchyma, limits lycopsid water use via low/high carbon

dioxide/water vapor sink strength. Lycopsids can be likely enhanced within Paleozoic atmospheric conditions due to higher carbon dioxide gas influx conductance.

The solar energy uptake of these plants is affected by the photosystem II organization and regeneration efficiency. The microphyll leaf structure has also been implicated in minimizing the photosynthetic surface area available for solar photosystem II activation (Beerling et al., 2001). Due to the morphological primitiveness of these plants, respective to angiosperm plants which photosynthetic models are based, it is reasonable that the maximal rate of electron transport (J_{max}) resulting from photosystem II activation of *H. lucidula* is unique. J_{max} is dependent upon the product of the light saturated potential rate of electron transport (j_{max}) and the superficial density of chlorophyll (Farquhar et al., 1980); j_{max} is dependent upon an optimal operational temperature that which exceeded preferentially leads to damage of chlorophyll a of photosystem I and consequently the chlorophyll A-B binding protein which connects photosystem I to photosystem II and stromal lamellae granum membranes- changing the optimal plant response wavelength (Armond et al., 1978). Differences within *H. lucidula* J_{max} could suggest differences in chlorophyll density or that there exist thermodynamic differences in the light harvesting complexes of lycopsids, consistent with changes in optimal operational temperature. While there is not specific evidence suggesting that there are differences in the organization of photosystem II between these and modern plants, the ability for these plants to manage temperature changes is related to the ability for plants to undergo leaf cooling transpiration.

The metabolic efficiency of these plants, like all organisms, is dependent upon the rate of its enzymes kinetics which are affected by temperature driven denaturation, water

utilization, and chemical reaction rates. Temperature-wise, *H. lucidula* is fairly hardy and is capable of surviving within modern cold environments of at least USDA hardiness zone 3b (corresponding to -35^{o}F to -30^{o}F) into 7a (corresponding to 0^{o}F to 5^{o}F). As previously discussed, while this could suggest a limitation during periods of high atmospheric carbon dioxide concentrations, as the consequent solar forcing would lead to global temperature increases which are may not be optimal for *H. lucidula*-like plants, the ability for like-plants to remain cool inner leaf temperatures would be unaffected by temperatures as transpiration rates would be unaffected by temperature; however, the consequently changes in atmospheric pressures due to gas composition could possibly further enhance transpiration rates alongside carbon dioxide influx by increased stomatal pore gas mixing (Graham et al., 1995). This suggests that the chemical availability of free carbon dioxide gas substrate is the most important factor in regulating these plants' metabolism, given that these plants are supplied with adequate solar PAR to the plant thylakoid lamella and enough water to keep guard cell's turgid.

The ability for a plant to take up nutrients is affected by the presence and type of symbiosis the plant has within its roots with nitrogen fixating rhizomal bacteria or fungi. This defines the source strength of this system. While the conductance of this system is limited by the types of vascular transport tissues available, the metabolic rates of the associated enzymes. Leaf nitrogen content has been previously associated with an increased electron transport capacity and associated superficial density of RuBisCO, consistent with a nutrient deficiency as nitrogen is the primary plant macronutrient due its inclusion in amino acids and role in general protein development (Farquhar et al., 1980; Voet, 2013). Curiously, while rhizomes have been observed within these plants, high

levels of fertilization have been found to be detrimental to the growth of clubmoss suggesting that these plants are adapted to growth in oligotrophic primarily inorganic mineral loam soils and do not require mycorrhizal or cyanobacterial association; the presence of organic matter within clubmoss biosol has been additionally found to release organic acids, effectively reducing nutrient buffering capacities and reducing the aeration capacity necessary for carbon dioxide gas uptake (Benca, 2014).

Pennsylvanian Ecological Conditions

The Pennsylvanian epoch of the late Carboniferous period has been proposed to have experienced several relatively short, several hundred thousand year, decreases in atmospheric moisture levels that progressively increased seasonal tropical drying and resulted in a reorganization of marshy wetland vegetation to that of dense tropical rainforests on a global scale (Dimichele et al., 2009). This change in global hydrologic cycling potentially lead to a geologically unprecedented climate change, wherein a period of global warming transitioned to a global ice age marked by oscillating planet-wide periods of intense glaciation and vegetative regrowth (Dimichele et al., 2009; Royer et al., 2004). The Pennsylvanian was generally amicable to current atmospheric conditions. While atmospheric carbon dioxide concentrations during the Pennsylvanian epoch were only 20 ppm higher than modern day levels of approximately 400 ppm (Tans and Keeling, 2016) the oxygen concentration of the Pennsylvanian epoch was roughly 10% higher (Berner, 2009; Came et al., 2007). Increased carbon dioxide levels have been implicated in climate change, but oxygen gas has not been previously implicated as a solar radiative-forcing greenhouse gas (Came et al., 2007; 2001). Previous work

acknowledges that changes in the composition of Earth's atmosphere have leads to changes in atmospheric pressures throughout deep-time (Graham et al., 1995).

In order to assess the effects of early vascular, non-seeding, plants to the unique conditions of the late Carboniferous, I grew the extant lycopsids in chambers with atmospheric conditions similar to previous descriptions of the period. Plants were grown in soil within diurnally lit individual chambers for at least eight weeks at near constant laboratory temperature and relative humidity. These chambers were selectively pressurized to 118.1 kPa and fed an enriched 30% oxygen air source, throughout the length of this experiment.

The effects of increased atmospheric pressure and oxygen treatment were characterized through morphological measurements in leaf morphology, surface stomatal morphology, subsurface stomatal morphology and physiology measurements in gas exchange, chlorophyll fluorescence, and ribulose-1,5-bisphosphate carboxylase/ oxygenase expression. Within this work, we examine the relationships between morphological characteristics and how these characteristics relate to physiological gas conductance. Additionally, we demonstrate that extant lycopsid stomatal dynamics are poorly modeled by current models and suggest a modified gas conductance model that considers subsurface leaf morphologies.

CHAPTER THREE

Materials and Methods

Experimental Design

For this study, I used *H. lucidula*- an extant member of the ancient Lycopodiophtya vascular plant sub-kingdom division. Live healthy plants were obtained from Carolina Biological Supply (Burlington, NC, USA). After acquisition, plants were grown in open air conditions for a three week period for acclimation then placed into the chambers. Sealed, pressure chambers were constructed from clear acrylic 2 liter chambers with hinged tops and rubber gaskets. In the top lid of each chamber, inlet and outlets ports were installed consisting of two Watts LFA-732 ¼" FIP couplings and LFA-96 hose barbs, fitted with four Hillman 880372 7/16" ID rubber washers, and sealed with thermoplastic adhesive. Each chamber was also outfitted with a Korky 450CM 7 cm ID flush valve replacement seal in order to provide a higher seal Approximately 0.5 m of NSF 61 grade tubing was used to attach the inlet port of each chamber to a central air source, regulated by air flow valves. Outlet ports of the chambers were fitted with a valve consisting of a single luer-lock connector connected to a single two-way calibrated exhaust valve (Appendix A).

For the experiments, 36 plants and chambers were divided into four treatment groups composed of nine individuals. These groups included the control (*C*), increased oxygen (*O*), increased pressure (*P*), and increased pressure and oxygen (*O+P*). The internal environment of chambers was each modified by controlling the source air inflow

and outflow rates of air. For all chambers, primary source air was from laboratory air supply that was bubbled through DI water before being fed into individual chambers in parallel for pressurization. This air supply flow rate was regulated in order to increase the inlet pressures.

Improvements in pressure chamber design were measured by the maximal obtainable chamber pressure and designed to reach the pressure conditions of previous descriptions of Paleozoic atmospheres (Table B.1).For the oxygen treatments, oxygen was mixed into the inlet air supply from a medical oxygen concentrator (Visionaire 5, AirSep Corp., Buffalo, NY, USA) at a rate of approximately 3.0 L min^{-1}. Chamber air pressure, oxygen, carbon dioxide, and relative humidity were monitored with inline barometers (SenSym SDX15A4, Vernier, Beaverton, OR, USA).

Non-pressurized treatments were maintained at 103.3 kPa, in order to allow the minimum flow rate for a calibrated air turnover; while increased pressure treatments chamber pressures were maintained at 118.1 kPa. Non-oxygenated pO2 levels were maintained at an ambient 21 %. The pO2 of increase oxygen treatments was maintained at 30 %. Each chamber was calibrated to a constant outflow of 0.5 L min^{-1} (QuBit System F1000 Flow Meter, Kinston, ON, Canada) to maintain a consistent mixing of air surrounding the plants between treatment chambers.

The elevated pressure chosen for this experiment (P_{a_j}; 118.1 kPa) can be estimated with respect to current atmospheric conditions, changing the concentration of a single atmospheric gas, here oxygen (Poulsen et al., 2015):

$$P_{a_j} = ((C_i \cdot P_{a_i}) - ((C_i \cdot P_{a_i} - C_j \cdot P_{a_i})/1\text{-}C_j))/C_j$$

where P_{a_i} is current atmospheric pressure at 24.4^{o}C (104.645 kPa), C_i is the current atmospheric gas concentration (21 %), and C_j is the prospectively changed atmospheric gas concentration (30 %). The value of P_{a_i} was calculated as an ideal gas at approximately 4^{o}C cooler from equatorial levels:

$$P_a = \rho_o/(MW_{dry\ air})\cdot RT$$

where ρ_o is the standard atmospheric density at 15^{o}C corresponding to 101.325 kPa (1.225 kg m^{-3}), $MW_{dry\ air}$ is the combined fractional molar mass of the atmosphere (28.967 g mol^{-1}), R is the gas constant (8.314,462,175 J mol^{-1} K^{-1}, Mohr et al., 2012), and T is temperature in Kelvin.

Plants were grown in small pots with normal potting soil and within pressure chambers for at least eight weeks at a near constant laboratory temperature of 22 ^{o}C. All chambers were maintained at an approximate consistent relative humidity of >80%. All plants were illuminated with fluorescent T12 growth lights with a diurnal light cycle from 08:00 to 22:00. Plants were watered regularly to maintain continuously moist soil; pressure treated plants required more frequent watering. Preliminary experiments found that *H. lucidula* grew two centimeters within a period of eight weeks. Therefore all measurements were collected from the proximal/top most two centimeters of shoots to account for pre- and post-treatment growth.

Post-Treatment Leaf Morphology

Post-treatment measurements of leaf morphology were taken by harvesting all leaves (approximately 100) from the top two centimeters of a single plant from each treatment.

The sampled leaves were flattened and affixed to a blank sheet of paper via translucent adhesive tape with care to avoid the overlap any whole leaves. These pages were digitally scanned at 600 dpi and individual leaf dimensions were determined using ImageJ (Schneider et al., 2012). The sum of all plant leaf areas was analyzed for outliers via ESD and individual leaf areas were symmetrically trimmed by 0.25Q, in order to remove spurious imaging artefacts. The individual leaf area, individual leaf aspect (length to width) ratio were then determined from these measurements.

Afterwards, previously affixed leaves were removed from the paper pages using 95 % ethyl alcohol. Leaves were placed into glass vials and dried at 80 °C in a gravity oven for 48 hours. The dried leaves were then weighed via an analytical balance to within 0.1 mg and the average specific leaf area per treatment calculated as the ratio of area to these mass measurements.

Surface Stomatal Morphology

Stomatal topology was characterized via optical imaging and subsequent image processing. Digital microscopy images were produced from leaf surface impressions of plant. Leaf surface impressions were produced from the top two centimeters of *H. lucidula* leaves following treatment at various atmospheric conditions, and not subject to gas exchange or fluorescence measurements. Leaf samples were coated in a thin layer of clear enamel on their abaxial sides and allowed to dry overnight. The enamel leaf impressions were then collected from the leaf samples, placed onto individual glass microscope slides, and covered with a cover slip. The individual leaf impressions were digitally imaged under an Olympus BH-2 (Shinjuku, Tokyo, Japan) light transmission microscope via an OMAX A35140U camera at 100X magnification.

Digital imaging of the enamel impressions from the sampled leaves in the microscope field of view were overlain with a digital 3 x 3 grid of boxes each 500 by 500 pixels (0.0169 mm^2) in size (Poole and Kürschner, 1999). The area of the impression with the highest concentration of stomata was placed within the center box of this grid by adjusting the microscopy stage for, generally centered between the leaf midrib and edge. Image measurements from the top left, center, and bottom right digital boxes were then recorded for each leaf. The purpose of this sampling was to account for concentration of stomata along the leaf midrib in *H. lucidula*.

From saved image data, pavement and guard cells were counted within the ImageJ software, counting only from three boxes across the grid central diagonal. This was done to account for the variable distributions of stoma down the length of the leaf. Next, the aperture size of each stoma within the image was digitally measured to the nearest 0.01 mm^2.

Stomatal density, number of guard cells per sampling area observed (D; m^{-2}), and index, the guard cell to pavement cell development bias (SI; %), values were calculated as (Aliniaeifard et al., 2014):

$$D = \frac{\text{total grid guard cells}}{2 \cdot \text{number grid boxes}}$$

$$SI = \frac{\text{stomatal density}}{\text{stomatal density} + \text{pavement cell density}} \cdot 100\ \%$$

The relatedness of *H. lucidula*'s D and SI were examined via least squares linear regression. This analysis was conducted in response to previous work analyzing the effect of SI alongside D (Beerling, 1998), despite evidence that SI is merely a less variable surrogate for D (Konrad et al., 2008).

Additionally, the effects of variable aperture size was upon a modeled physiological response was analyzed. Stomatal water vapor conductance values ($g^{s}_{H_2O}$; mmol m^{-2} s^{-1}) were calculated by (Franks and Farquhar, 2001) from these surface morphologies:

$$g^{s}_{H_2O} = \frac{d \cdot D \cdot a_{max}}{M_V\left(l_p + (\pi/4) \cdot \sqrt{a_{max}/\pi}\right)}$$

where *d* is the diffusivity of water within air (m^2 s^{-1}), *D* is stomatal density (m^{-2}), a_{max} is the maximum aperture size (m^2), l_p is pore depth (m), and M_V is the molar volume of air (m^{-3} mol) at 22 ^oC. The value of *d* in moist air was calculated by (Bolz and Tuve, 1973):

d = -2.775 x 10^{-6} + 4.479 x 10^{-8} · (22^{o}C + 273.15 ^{o}C)

+ 1.656· 10^{-10} (22^{o}C + 273.15 ^{o}C)

Pore depth values were assumed for *H. lucidula*, due to the lack of previous literature detailing lycopsid gas exchange dynamics. Although this calculation is similar to previous work, this does not assume a diffusion shell as a part of the pore depth (Konrad et al., 2008). The pore depth was calculated as an average between the radius of a_{max} and half a representative plant cell breadth of 50 μm (c_b; m) (Fanourakis et al., 2015):

$$l_p = \frac{\frac{c_b}{2} \cdot \sqrt{a_{max}/\pi}}{2}$$

Stomatal conductance values were converted from water vapor transport to diffusively equivalent free carbon dioxide gas values by (Nobel, 2009):

$$g_{CO_2} = g_{H_2O} \cdot (D_{CO_2}/D_{wv})$$

where D_{CO_2} is 1.56 x 10^{-5} m^2 s^{-1} and D_{wv} is 2.50 x 10^{-5} m^2 s^{-1} at 25^{o}C.

The degree of operational stomatal conductance ($g_{s,op}$) was graphically estimated as the ratio (φ_{g_s}) between modeled average aperture (a_{mean}) to modeled a_{max} stomatal conductance (Fanourakis et al., 2015):

$$\varphi_{g_s} = \frac{g_{s,mean}}{g_{s,max}} = \frac{a_{mean}}{a_{max}} \cdot \frac{\left(\left(\frac{c_b}{2}\sqrt{a_{max}/\pi}\right)/2 + (\pi/4) \cdot \sqrt{a_{max}/\pi}\right)}{\left(\left(\frac{c_b}{2}\sqrt{a_{mean}/\pi}\right)/2 + (\pi/4) \cdot \sqrt{a_{mean}/\pi}\right)}$$

$$g_{s,op} = \varphi_{g_s} \cdot g_{s,max}$$

Post-Treatment Subsurface Stomatal Morphology

Stomatal conductance models require stomatal pore depth values that necessitated transverse cross-section imaging of *H. lucidula*'s stomatal complex. A modified Transmission Electron Microscopy (TEM) technique was used assess the stomatal characteristics in more detail. Post-treatment *H. lucidula* leaves, were collected from the top two centimeters of shoot tips and bottom two centimeters above the soil line, before gas exchange or fluorescence measurements. Leaf samples were prepared for sectioning following TEM tobacco leaf procedure.

Leaf samples were first submerged in 2.5 M glutaraldehyde in stock 0.06 M PO4 buffer pH = 7.2 for one hour in order to fix leaf proteins. This was followed by four 10 minute washes in buffer. Samples were then added to 2 % osmium solution in stock buffer for 90 minutes for fatty acid fixation; following this, leaves took on a black 'burnt' appearance. Another set of four 10 minute buffer washes washed the samples of excess osmium solution. Leaves were then dehydrated in sets of two ethanol washes of increasing concentration- 50 %, 70 %, 90 %, and 100 % for 10 minutes each wash. Afterwards, dehydrated leaves were washed in 1:1 ethanol:propylenoxide for 10 minutes,

followed by another 10 minute wash in 100 % propylenoxide. EMBED 812 resin was prepared fresh for each next resin exchange- leaves were exchanged in 1:2 resin:propylenoxide for more than one hour, followed by a 1:1 resin:propylenoxide for more than two hours, 2:1 resin:propylenoxide for more than three hours, and finally in 100 % resin for more than four hours. Note that the length of these exchanges allows for a natural stopping point for overnight exchange. Leaves sat overnight for the 1:1 resin:propylenoxide exchange. Each previous step was conducted at room temperature and samples were kept on a slow spinning carousel in between washes and exchanges. The final embedded leaf samples were poured into 100 % resin and placed into a 60 ^{o}C oven for 48 hours in order to allow resin polymerization.

Resin slabs were trimmed via Leica EM Trim 2 and leaves were transversely sectioned transversely via Leica Ultracut EM UC7 microtome to widths of 4000 nm. Following analysis of substomatal cavity features, further sectioning was conducted via CryoStar NX50 Cryo-microtome at 40μm, in order to verify the tissue organization observed within resin semi-thin sections. The 4000 nm semi-thin sections were subsequently placed unto glass, mounted to sample studs via carbon tape, grounded with silver paste, and sputter coated in 20 nm gold via Leica ACE600 in order to allow verify the internal leaf tissues via Scanning Electron Microscopy (SEM). Leaf stomatal cross-sections were imaged via FEI Versa 3D low vacuum FIB-SEM cursorily at 300X, 10.0 kV, 5.5 spot size, and 10.00 mm working distance and in detail at 1500X, 10.0 kV, 5.5 spot size, and 4.00 mm working distance.

Development of a Modified Stomatal Conductance Model

Using transverse leaf sections, I identified and measured characteristics of *H. lucidula*'s unique sub-stomata morphology. From this information, I defined a new stomatal conductance model, similar to previous work on stomatal crypts, including: the stomatal ledge aperture conductance (g_{LA}), stomatal outer cavity conductance (g_{OC}), stomatal throat conductance (g_T), and substomatal cavity conductance (g_{SSC}) (Heinsoo, 1999; Metcalfe and Wilkerson, 1979). I considered that diffusion shells exist between the boundary layer, leaf surface, and substomatal layers with varying conductance.

This morphology defines four openings that may constrict gas exchange in *H. lucidula* leaves including: 1) the ledge aperture, which consists of a stomatal aperture width (AW) and the average depth of both sides of the stomatal ledge (L1 and L2), 2) an outer (cavity) aperture, which consists of the area of the outer stomatal cavity of a certain width (OC) and depth (OD), 3) the throat (aperture), which consists of the size of the stomatal throat (ST) and throat depth (TD) and 4) the substomatal cavity with a horizontal width (SSCH) and vertical depth (SSCV).

The area of each of these constrictions was considered an ellipse- one radius being half the diameter of each the ledge aperture, outer aperture area, stomatal throat, or substomatal cavity width; the other being half of c_b. Conductance of these separate structures was calculated by substituting a_{max} and l_P into the denominator of Franks and Farquhar (2001) model. For example g_{LA} was calculated by:

$$g_{H_2O}^{LA} = \frac{d \cdot D \cdot a_{max}}{M_V\left(\left(\frac{L1 + L2}{2}\right) + \left(\pi/4\right) \cdot \sqrt{\left(AW \cdot \frac{c_b}{2}\right)}\right)}$$

Old leaf conductance values were calculated from pre-treatment stomatal surface measurements, while new leaf conductance values were calculated from post-treatment measurements.

These structures are in series and form a stomatal pore conductance (g_{pore}). This is in parallel with cuticle conductance (g_{cut}) and defines the epidermal conductance (g_{epi}). This g_{epi} value is in series with the boundary layer conductance (g_b) as a surface conductance (g_{sur}).

$$g_{pore} = \left(\frac{1}{g_{LA}} + \frac{1}{g_{OC}} + \frac{1}{g_T} + \frac{1}{g_{SSC}}\right)^{-1} \approx g_s$$

$$g_{sur} = \frac{g_b(g_{pore} \cdot \varphi_{g_s} + g_{cut})}{g_b + g_{pore} \cdot \varphi_{g_s} + g_{cut}} = \frac{g_b(g_{epi})}{g_b + g_{epi}} \approx g_l$$

The leaf boundary layer conductance (g_b; mol m^{-2} s^{-1}) was derived from measurement of the leaf width (w; in m) and calculated by (Campbell and Norman, 1998):

$$g_b = 0.110\sqrt{(u/0.72w)}$$

where *u* is a representative wind speed in m s^{-1}. Leaf boundary layer conductance was calculated using a representative wind speed of 0.2 m s^{-1}.

Leaf cuticle conductance (g_{cut}; mol m^{-2} s^{-1}) was estimated by:

$$g_{cut} = g_{min}/M_V$$

where g_{min} is the maximal possible minimum cuticle conductance velocity in m s^{-1} and M_v is the molar volume of air in m^3 mol^{-1}. A representatively large minimum leaf cuticle conductance value of cold tolerant needle tree leaves was divided by atmospheric density (control 0.02422 m^3 mol^{-1}, pressure 0.02163 m^3 mol^{-1}) and converted into mol CO_2 (Anfodillo et al., 2002).

The g_s values derived from the CID-340 are automatically calculated using a set boundary layer conductance of 3.33 mol m^{-2} s^{-1} as part of the instrument design. To compare conductance values derived from microscopy estimates, I removed this boundary layer conductance value and recalculated an infrared gas analyzer (IRGA) $g^{l}_{H_2O}$. These IRGA values were only due to gross gas exchange and calculate g_l, without using g_{cut} and g_b values.

IRGA Measured Physiology

Gas exchange measurements of individual leaves was not possible due to the relatively small microphyll leaves relative to volume of the cuvette, I estimated a cumulative leaf area taken from the top two centimeters of each plant shoot from a subset of four separate non-chambered plants. All leaves were removed from the top two centimeters of each plant, scanned, and imaged for area as described previously (Schneider et al., 2012). These leaves were used to derive a mean cumulative leaf area. This mean cumulative leaf area was used as input for gas exchange measures of plant shoots within the instrument cuvette.

IRGA measurements were taken from the top two centimeters of each plant shoot. Measurements of CO_2 and H_2O vapor flow were measured from each plant before and after treatment via a CID CI-340 Hand-held Photosynthesis System (CID Bio-Science, Inc., Camas, WA, USA). This produced the average gas exchange rates of photosynthesis (Pn; μmol m^{-2} s^{-1}), transpiration (E; mmol m^{-2} s^{-1}), conductance to water vapor ($g^{s}_{H_2O}$; mmol m^{-2} s^{-1}), and internal CO_2 (C_i; ppm) across leaf surfaces at laboratory atmospheric pressures of 99 kPa to 102k Pa and temperature of 22^{o}C.

Light adapted leaf fluorescence was also measured in the top two centimeters of stems with the addition of a CID CI-510CF fluorescence module in response to a red light LED of 0.25 µmol m^{-2} s^{-1} at a distance of 12 mm from the leaf surface. Measurements were taken at a minimum one day following gas exchange measurements to prevent plant stress. Chlorophyll pulse-amplitude-modulation fluorescence spectroscopy allowed the quantum yield efficiency of photosystem II (ΦPSII) to be calculated, via the function of light-adapted plant leaf 'flash' maximal (F'_m) and steady state (F_t) fluorescence. This was multiplied by the gas exchange amount of Photosynthetically Active Radiation (PAR; µmol m^{-2} s^{-1}), the absorptivity of plant chlorophyll a (84%), and a ratio split of 1:1 between PSI (P700 reaction center) and PSII (P680 reaction center), to calculate the electron transport rate also known as J (ETR; µmol m^{-2} s^{-1}) (Maxwell and Johnson, 2000; Flexas et al., 1998):

$$\Phi PSII = (F'_m - F_t)/F'_m$$

$$ETR = PAR \cdot \Phi PSII \cdot 0.84 \cdot 0.5$$

From these data, I calculated PAR Light Use Efficiency (PLUE; g_c MJ^{-1}), instantaneous Water Use Efficiency (WUE), and stomatal/intrinsic WUE (WUE_i) (Medlyn, 1998; Soni et al., 2012; Medrano et al., 2015):

$$PLUE = (Pn/PAR) \cdot (MW_C \cdot 550\ nm)/(N_{A\gamma} \cdot h \cdot c) \cdot (10^{-3}\ m\ J\ nm^{-1}\ MJ^{-1})$$

$$WUE = (Pn/E) \cdot 10^{-3}\ \mu mol\ mmol^{-1}$$

$$WUE_i = (Pn/g_{H_2O}) \cdot 10^{-3}\ \mu mol\ mmol^{-1}$$

where, MW_{CO_2} and MW_C is the molecular weight of carbon dioxide and carbon in g mol^{-1}, N_A is Avogadro's number, γ indicates photons, h is Planck's constant in J s^{-1}, c is the

speed of light in m s^{-1}. At 550nm this relationship can be used to calculate PLUE from the ratio of Pn to PAR as multiplier of 55.172 g_C μmol_γ MJ^{-1} μmol_{CO_2}.

Post-Treatment Ribulose-1,5-bisphosphate Carboxylase/Oxygenase

The quantification of plant leaf Ribulose-1,5-bisphosphate Carboxylase/ Oxygenase (RuBisCO) concentrations required that samples were collected and extracted protein solubilized cold to prevent sample degradation due to protease activity. Although anecdotal as given common practice to freeze-thaw protein standards within molecular laboratories, I found it acceptable to use slow-frozen plant material samples. This procedure has been substantiated by other researchers, finding that slow freezing produces smaller ice-crystals and is ideally followed by fast thawing, whereas the opposite produces protein damage (Cao et al., 2003; Cuhadar et al., 2013). Additionally, cryogenic studies have demonstrated that although lipid arrangements are damaged by freezing, the denaturation profiles of proteins do not show substantial change when kept at -20 ^oC, while permanent cold-denaturation damage does occurs at -80 ^oC 'deep freeze' cold storage (Bischof et al., 2002; Wolkers et al., 2007).

Since *H. lucidula* leaves are small, whole leaves and stems were used for analysis to provide sufficient mass for analysis. *H. lucidula* stems following treatment at various atmospheric conditions, and not subject to gas exchange or fluorescent treatment, were collected and slow frozen in a -20 ^oC freezer. The top two centimeters of shoot tips and bottom two centimeters above the soil line was cut from frozen samples, separated, weighed, and processed via copious cold liquid nitrogen. This allowed sample cell walls to be broken using a cold mortar and pestle, as well as preventing sample degradation due

to protease activity (Ma et al., 2009; Rouhani et al., 1973). The majority of samples were found to weigh less than 500 mg.

Samples were ground to a fine powder and suspended in 500 µL room temperature 1X CHS-PBS. An initial stock of 10X CHS-PSB was prepared to 1.37 M NaCl, 27 mM KCl, 100 mM Na_2HPO_4,18 mM KH_2PO_4, and a final pH of 7.4 (2006). Samples were spun 5 minutes at 10,000 rpm in an Eppendorf 5417R Centrifuge and 50 µL of the supernatant was used for analysis at room temperature. Competitive Enzyme-linked immunosorbent assay (ELISA) was conducted as it presented many advantages over similar techniques: minimizing the preparation of neurotoxic gels, does not require prior UV Bradford standardization, and the high sensitivity of ELISA procedure allowed complex-mixture samples to be analyzed, minimizing the need for sample dilution and purification techniques that effect recovery rates. Competitive ELISA produces an unambiguous signal that is detectible depending on the conjugation of the secondary antibody, as unbound and bound antibodies will precipitate different molecules that are visible in the light spectrum. RuBisCO standard, polyclonal anti-RuBisCO primary antibody, and HRP-conjugate secondary antibody were purchased as a kit (MyBioSource, Inc., San Diego, CA, USA; cat: MBS281711). Sample wells were incubated for one hour at 37 ^{o}C with HRP-conjugate, cleaned 5 times, and again incubated for 10 minutes at 37 ^{o}C, stopping with acid when the standard ladder was a deep blue.

ELISA signal was measured on a BioTek ELx800 microplate reader at 450 nm, zeroed to 540 nm. The standard signal was fit to a four parameter logistic curve. The recovered µg/mL RuBisCO signal was expressed on a per gram basis using the mass of initial plant material analyzed.

Data Analysis

The CI-340 photosynthesis, transpiration, and stomatal conductance data were found to be lognormal distributed and were transformed for analysis. The average gas exchange data for each plant was compiled by before and after each treatment and tested for normality via a sample size dependent Shapiro-Wilk statistic between each treatment group. Histograms which did not pass the S-W critical test statistic were analyzed for outliers, whereby any outliers visible within 95% CI box-whisker plots were tested against a general Extreme Studentized Deviate test for exclusion. Trimmed groups were consequently tested for normality via a non-tail heavy Kolmogorov-Smirnov test statistic. Whenever possible, pre-average 'raw' data was analyzed for outlier presence within data groups which did not meet the critical value, prior to trimming average plant data. Additionally, groups which were still not found to express normality or could not be trimmed of outliers, nonparametric Kruskal-Wallis tests were used to establish that these were similar to groups with normal distributions before and after data treatments. Gas exchange conductance values that were larger than Farquhar average stomatal aperture conductance values, representing the average maximum potential conductance, were excluded from analysis and assumed to be a result of instrumental error.

Data were transformed, for two-point (repeat measures) univariate ANOVA to test for significant ($p \leq 0.05$) change due to treatment within treatment groups, as the natural log of the absolute value of the ratio of post-treatment to pre-treatment data plus one. An alpha value of 0.05 was used for all analysis and all post-hoc analysis was conducted via Tukey's HSD.

Univariate ANOVA analysis was used in order to analyze data on a plant by plant treatment basis. This allowed the visualization of the effects of treatment between treatments, as preliminary analysis found significantly high physiological variance within treatment groups. Additionally, this analysis is better suited to my experimental method whereby plants were treated separately in individual chambers rather than exposed to treatment conditions within a large growth chamber. Hence, pooled treatment analysis was not conducted for physiological measurements. The surface stomatal morphological data was examined in a similar manner to allow relation between morphologically-based models to gas exchange physiological data.

Leaf morphology analysis between post-treatment leaves and RuBisCO analysis between pooled post-treatment new and old growth leaves were conducted via Welch's T-test. No data normalization or trimming was conducted for these analyzed as normality is not required for this test. This method was chosen since these samples were taken from the same plant and not compared in response to treatment over time, as the physiology was analyzed.

CHAPTER FOUR

Results

Post-Treatment Leaf Morphology

New growth leaves showed significant change in leaf dimensions following treatment compared with control values (Table 4.1). I found leaf area and width was smaller for all treatments relative to *C*. Yet, the effect of *O and O+P* upon leaf width was found to be significantly different from and almost two times the effect of *P*. Similarly, the *P* and *O* treated plants had smaller aspect ratios compared to *C*; while the aspect ratio of *O+P* treated plant leaves were not different from *C*. Additionally, the effect of *P* upon leaf aspect ratio was found to be significantly different from and more than two times the effect of *O*. In contrast, the mean SLA of *O* and *P* treated plants were significantly higher compared to *C*, whereas *O+P* plants had lower SLA values. Each SLA value was found to significantly differ from every other treatment.

Table 4.1 – The mean ± one standard deviation *(sample size)* leaf response of new growth *H. lucidula* specimens in response to treatment, detailing: individual leaf area, individual length to width, and tip specific leaf area. Superscript letters indicate values which were found to change significantly ($p \leq 0.05$).

Measure	*C (100)*	*P (102)*	*O (119)*	*O+P (105)*
Leaf Area (cm^2)	0.0457 ± 0.0093 [a]	0.0334 ± 0.0100 [b]	0.0320 ± 0.0076 [b]	0.0317 ± 0.0086 [b]
Leaf Width (cm)	0.0973 ± 0.0105 [a]	0.0901 ± 0.0125 [b]	0.0842 ± 0.0105 [c]	0.0835 ± 0.0102 [c]
Aspect Ratio (L:W)	5.5573 ± 0.8306 [a]	4.8985 ± 1.2921 [b]	5.2737 ± 1.2565 [c]	5.3727 ± 1.2488 [a]
SLA ($m^2 g^{-1}$)	0.0167 ± 0.0000 [a]	0.0221 ± 0.0000 [b]	0.0193 ± 0.0000 [c]	0.0162 ± 0.0000 [d]

Surface Stomatal Morphology

Surficial leaf microscopy showed that *H. lucidula* stomata were arranged in parallel lines between the midline and margin, while the stomatal subsidiary cells were arranged in an anomocytic pattern. Surface stomatal morphological characteristics were unchanged between treatments. Overall, *H. lucidula* was found to have a SI of 2.29 ± 0.57 %, SD (50); D of $9.61 \times 10^{-5} \pm 2.10 \times 10^{-5}$ μm^{-2}, SD (54); a_{max} of 546.79 ± 136.94 μm^2, SD (54); and a_{mean} of 349.27 ± 67.30 μm^2, SD (54) (Table 4.2).

Table 4.2 – The mean ± one standard deviation *(sample size)* surface stomatal of pre-treatment and post-treatment new growth of *H. lucidula*, detailing: stomatal index, stomatal density, maximal stomatal aperture area, and mean stomatal aperture area.

Treatment	Measure	Pre-treatment	Post-treatment
C (6)	SI (%)	2.16 ± 0.87	2.68 ± 0.41
	D (μm^{-2})	$8.05 \times 10^{-5} \pm 2.75 \times 10^{-5}$	$10.5 \times 10^{-5} \pm 1.84 \times 10^{-5}$
	a_{max} (μm^2)	462 ± 165	484 ± 152
	a_{mean} (μm^2)	278 ± 65.2	319 ± 98.3
P (7)	SI (%)	2.22 ± 0.69	2.38 ± 0.46
	D (μm^{-2})	$9.74 \times 10^{-5} \pm 2.96 \times 10^{-5}$	$9.74 \times 10^{-5} \pm 1.34 \times 10^{-5}$
	a_{max} (μm^2)	629 ± 169	589 ± 123
	a_{mean} (μm^2)	391 ± 81	357 ± 58
O (6)	SI (%)	2.06 ± 0.52	1.98 ± 0.42
	D (μm^{-2})	$8.88 \times 10^{-5} \pm 1.08 \times 10^{-5}$	$8.55 \times 10^{-5} \pm 1.19 \times 10^{-5}$
	a_{max} (μm^2)	497 ± 66	535 ± 107
	a_{mean} (μm^2)	351 ± 43	358 ± 65
O+P (7)	SI (%)	2.20 ± 0.61	2.64 ± 0.36
	D (μm^{-2})	$10.1 \times 10^{-5} \pm 2.40 \times 10^{-5}$	$10.8 \times 10^{-5} \pm 1.61 \times 10^{-5}$
	a_{max} (μm^2)	555 ± 104	576 ± 151
	a_{mean} (μm^2)	366 ± 40	354 ± 37

Stomatal index and stomatal density for both pre-treatment and post-treatment plants were found to be moderately linearly correlated (Figure 4.1). The observed

relationship between stomatal index and density is similar in slope between pre- and post-treatment values. This seems to indicate that this result is fairly consistent in capturing the distribution trend. However, there was an almost two magnitude difference between pre- and post- treatment y-intercepts. The closeness of the pre-treatment y-intercept of 0.00126 to zero suggest that the pre-treatment correlation is fairly reasonable, considering that without the presence of stomata neither a stomatal density or index value are capable of being larger than zero. Moderate correlations were found between a_{mean} and a_{max}. Following this result, I report *H. lucidula*'s φ_{gs} as between 0.496 and 0.651 (Figure 4.2).

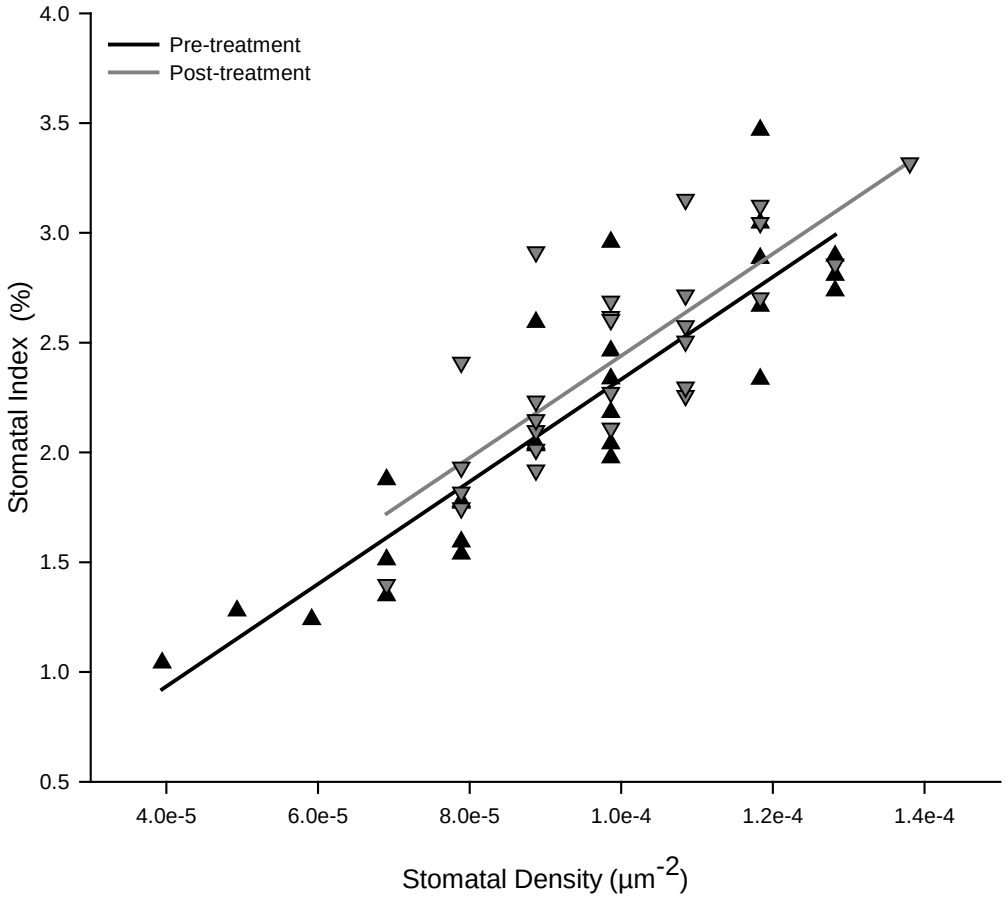

Figure 4.1 – Values of stomatal density and stomatal index for pre-treatment (y = 0.00126 + 23300x) and post-treatment (y = 0.118 + 23200x) leaves of *H. lucidula*. Least squares linear regression models respectively were calculated with r^2 values of 0.80 and 0.66.

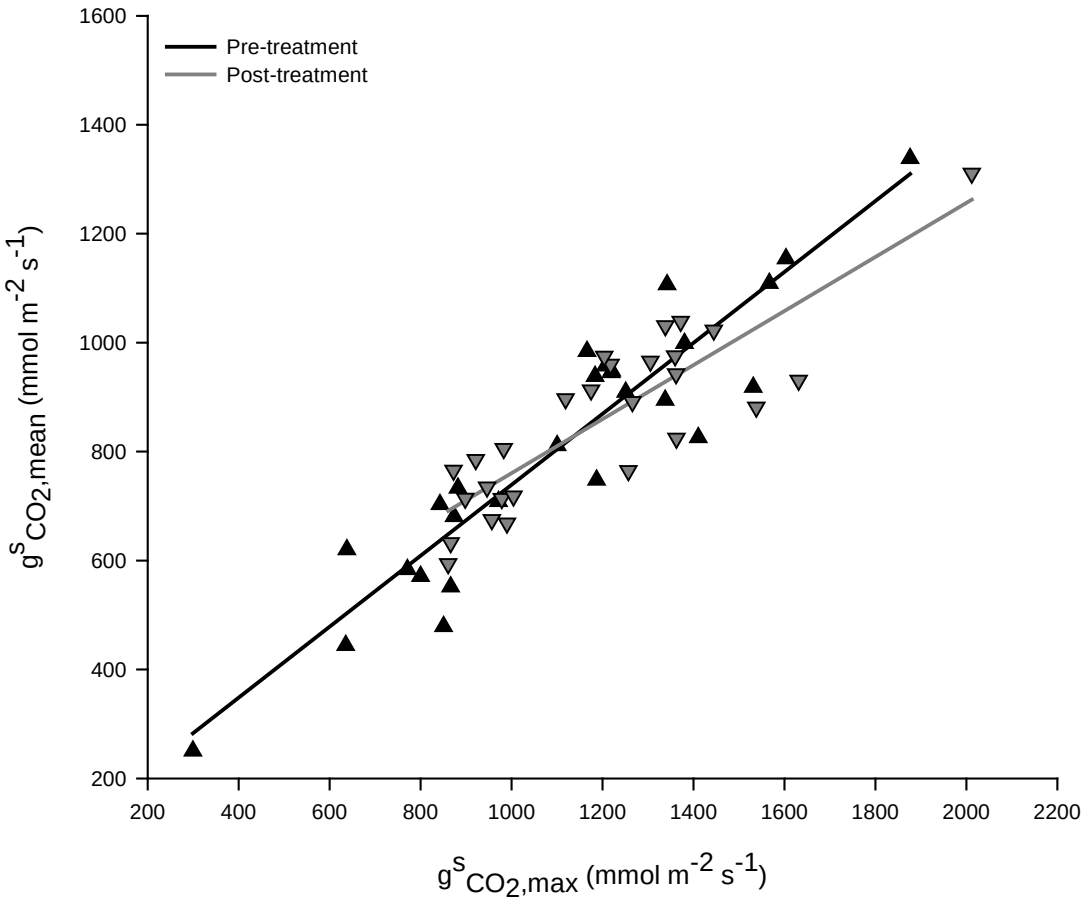

Figure 4.2 – Values of modeled a_{max} and a_{mean} stomatal conductance for pre-treatment (y = 88 + 0.651x) and post-treatment (y = 264 + 0.496x) leaves of *H. lucidula*. Least squares linear regression models respectively were calculated with r^2 values of 0.87 and 0.74 to estimate the pore size dependent degree of operational stomatal conductance (φ_{g_s}).

Post-Treatment Subsurface Stomatal Morphology

Surface bright-field microscopy suggested the presence of prominent guard cell outer ledges confirmed by TEM of individual stomata transverse sections. Transverse sections confirmed the presence of diminutive inner ledges and that stomatal pores are level with the leaf surface, not exhibiting any 'sunken' crypt, cup, or rampart morphology. The average dimensions of subsurface stomatal morphology in pooled old and new leaves following treatment are reported (Table 4.3).

Table 4.3 – Stomatal complex cross-sectional morphologic features of pooled old and new leaves following treatment. All measurements here consider an observer relative to the leaf surface, reported as either diameters of a leaf subsurface stomatal cavity diameter (AW, OC, ST, SSCH) or its depth (L1/L2, OD, TD, SSCV). I report $l_{p,ts}$ values as the sum of transverse section derived OD and TD measurements.

Dimension (μm)	*C*	*P*	*O*	*O+P*
AW (aperture width)	2.93	3.91	5.88	4.92
L1 (ledge 1 depth)	2.17	1.59	1.71	2.63
L2 (ledge 2 depth)	2.415	1.58	1.79	2.38
OC (outer cavity width)	8.70	10.24	12.06	11.92
OD (outer cavity depth)	7.78	7.43	6.91	7.63
ST (stomatal throat width)	4.07	1.89	2.67	2.90
TD (throat depth)	12.89	15.59	15.34	14.23
SSCH (SSC width)	41.99	52.69	43.54	43.16
SSCV (SSC depth)	17.84	13.40	19.34	11.74
$l_{p,ts}$ (equivalent pore depth)	20.67	23.02	22.25	21.86

Development of a Modified Stomatal Conductance Model

I suggest that my subsurface measurements define a generic lycopsid leaf opening. I defined *H. lucidula*'s stomatal conductance partwise from these morphological measurements in terms of g_{LA}, g_{OA}, g_T, and g_{SSC}. These g_{CO_2} were compared to measured IRGA values and φ_{g_s} corrected Franks and Farquhar (2001) model values, based only on surface stomatal morphology measurements (Table 4.4). Comparison of the conductance based on the Franks and Farquhar modeled conductance values showed a poor fit IRGA data, relative to my proposed g_{pore} model (Figure 4.3). Regardless of treatment, my g_{pore} model most closely approaches the 1:1 IRGA line.

Table 4.4 – Stomatal conductance measurements derived from subsurface stomatal measurements of pooled old and new leaves. These measurements yielded stomatal pore conductance values which were used to derive leaf (surface) conductance values.

Conductance (mol m^{-2} s^{-1})	*C*	*P*	*O*	*O+P*
$g_{H_2O}^{LA}$ (ledge aperture)	6.72	9.63	4.79	8.20
$g_{H_2O}^{OC}$ (outer cavity)	1.96	2.70	1.55	2.66
$g_{H_2O}^{T}$ (throat)	1.94	2.94	1.68	3.04
$g_{H_2O}^{SSC}$ (substomatal cavity)	0.86	1.27	0.76	1.50
$g_{CO_2}^{pore}$ (combined pore)	0.15	0.22	0.13	0.24
IRGA g_l (instrument)	0.0201	0.0212	0.0211	0.0639
Franks and Farquhar	0.4334	0.5573	0.3999	0.5799
$g_{CO_2}^{sur}$ (combined models)	0.1385	0.1991	0.1234	0.2129

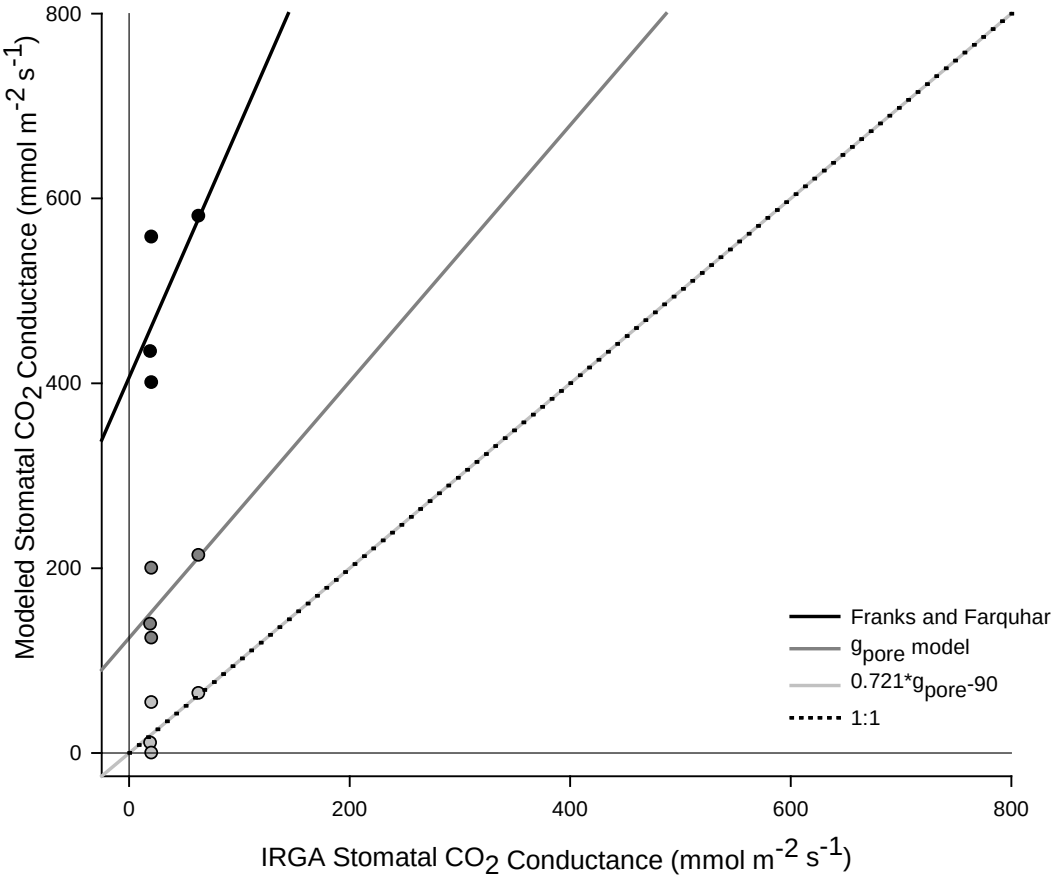

Figure 4.3 – Comparison of pooled pre-treatment and post-treatment average IRGA g_l measurements to g_l values calculated from the Franks and Farquhar (2001) model using only surface stomatal morphology (y = 407 +2.73x), my developed g_{pore} model (y = 125 +1.39x), and 1:1 corrected g_{pore} model (y = 0.0014 +1.00x). Least squares linear regression models respectively were calculated with r^2 values of 0.43 and 0.46.

IRGA Measured Physiology

The mean cumulative leaf area for the top two centimeters of plant shoot tips was determined to be 5.77 cm^2 ± 0.66 cm^2, SD. This numbered was derived from 534 leaves taken from a subset sample population of four non-chambered plants. This shoot leaf area value was used for IRGA measurements. Individual leaves had: an average area of 0.0465 cm^2 ± 0.0093 cm^2, SD; average width of 0.1154 cm ± 0.024 cm, SD; and an aspect ratio of 3.8160 ± 1.2103, SD.

Gas exchange stomatal conductance and internal CO_2 levels and fluorescent photosystem II quantum yield were found to change significantly from C (Figure 4.4). Pre- and post-experimental log transformed photosynthesis and transpiration measurements were not significantly different within or among treatment; I report *H. lucidula*'s photosynthesis rate and transpiration rate as 1.40 ± 0.86, SE (50) µmol m^{-2} s^{-1} and 1.18, 0.85, SE (40) mmol m^{-2} s^{-1}, respectively (Table D.1). ANCOVA covariance matrix contrast analysis was conducted upon $g^{s}_{CO_2}$ values in order to account for the miniscule yet significant changes in measurement atmospheric pressures (p = 0.017649) and air temperature (p = 0.013982), (p = 0.004377). This analysis indicated that the $g^{s}_{CO_2}$ of *P* plants was significantly higher than in *C* plants, and both *P* and *O* values significantly differed from *O+P* treated plants. C_i values were significantly higher in *O+P* plants, from 163.68 ± 20.8430 ppm, SE (8) to 266.100 ± 52.106 ppm, SE (8) despite every other treatment having lower post-treatment values. Chlorophyll fluorescence indicates that the organization of PSII was only significantly lowered from 0.69 ± 0.07, SE (8) to 0.27 ± 0.08, SE (8) due to *P*.

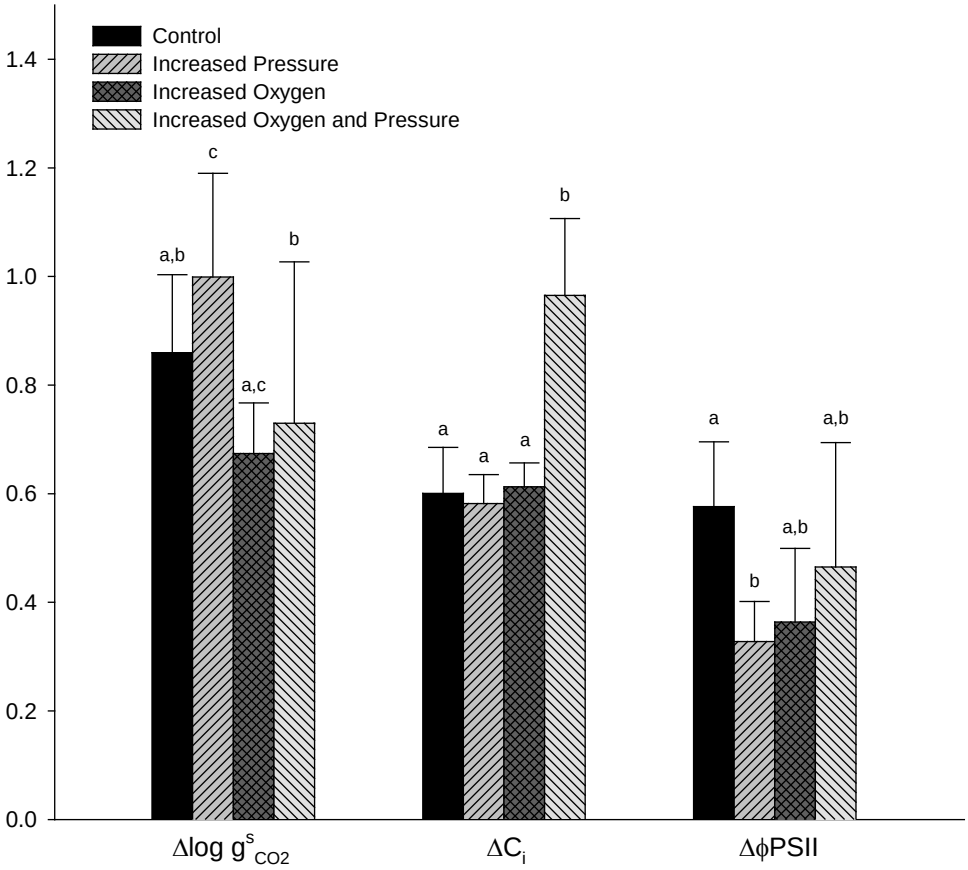

Figure 4.4 – Error bars indicating standard error of change, reported as the natural log of absolute value of the ratio of post-treatment to pre-treatment data plus one. The change of *H. lucidula* gas exchange and fluorescence in response to various atmospheric conditions details ANCOVA-tested stomatal CO_2 conductance, internal CO_2, and photosystem II organization in response to various atmospheric conditions. Different letters indicate significant differences ($p \leq 0.05$).

The combined physiological parameters of ETR and WUEi and were found to change significantly from *C* (Figure 4.5). ETR was found to have significantly lowered from 129.42 ± 26.03 µmol m^{-2} s^{-1}, SE (8) to 39.62 ± 3.07 µmol m^{-2} s^{-1}, SE (8) due to *P*. WUEi was also found to significantly different due to *O+P*; additionally, WUEi was higher following *O+P* from 0.0310 ± 0.0311, SE (4) to 0.0504 ± 0.0369, SE (4), while all other treatments caused post-treatment values to be lower. PLUE levels following treatment were not significantly different from *C*, but the effect of *P* was found to significantly differ from *O* and *O+P*. WUE was also not found to differ due to treatment.

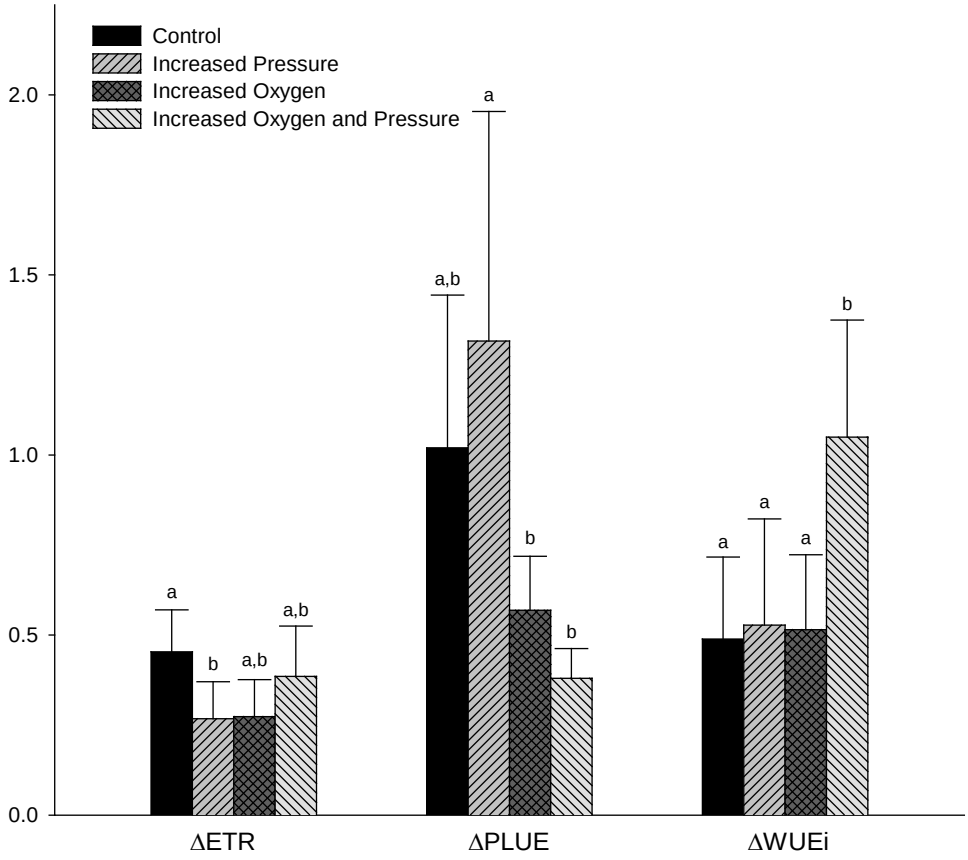

Figure 4.5 – Error bars indicating standard error of change, reported as the natural log of absolute value of the ratio of post-treatment to pre-treatment data plus one. The change of *H. lucidula* combined physiological parameters in response to various atmospheric conditions details linear electron transport rate, PAR light use efficiency, and intrinsic water use efficiency in response to various atmospheric conditions. Different letters indicate significant differences ($p \leq 0.05$).

Post-Treatment Ribulose-1,5-Bisphosphate Carboxylase/Oxygenase

Mass normalized expression data was fit to a four parameter logistic calibration curve of equation $\frac{1.52080+0.03493}{1+\frac{x}{17.28866}^{0.72122}} - 0.03493$ with $r^2 = 0.98$. RuBisCO expression was significantly different in *P* and *O+P* from *C* treatments. There were no significant differences in RuBisCO expression between *P, O,* or *O+P* treatments (Figure 4.6).

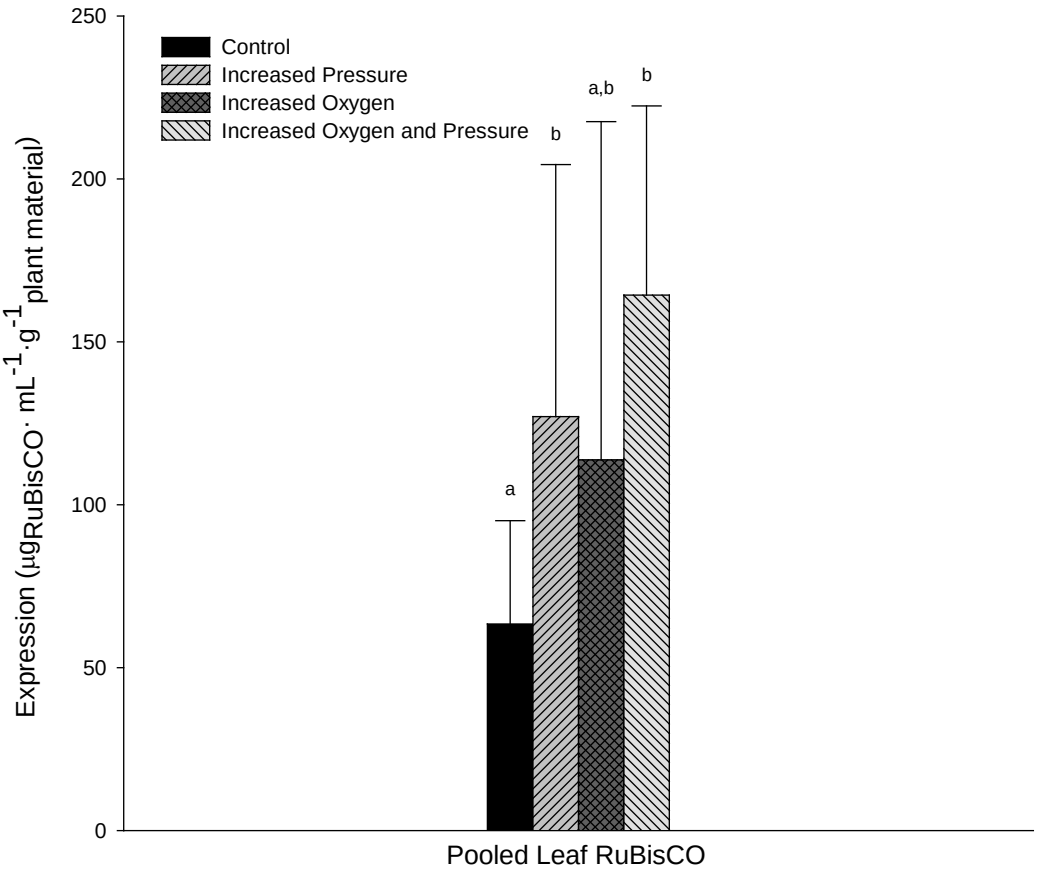

Figure 4.6 – Pooled means of new and old growth leaves following treatment. Error bars indicating one pooled standard deviation. Letters indicate significant differences ($p \leq 0.05$).

CHAPTER FIVE

Discussion

Post-Treatment Leaf Morphology

Changes in atmospheric conditions were found to affect leaf area, width, aspect ratio, and SLA of individual leaves. Plants exposed to both higher atmospheric pressure and oxygen had lower individual leaf areas and widths; yet, the effects of both increased atmospheric pressure and oxygen were not found to further lower leaf area in *O+P*, while the addition of oxygen led to significantly smaller leaf widths in *O* and *O+P* than *P*. This indicates that the morphological response to higher atmospheric pressure may be associated with an independent mechanism than oxygen. This resulted in leaf cell sizes that were smaller in response to higher atmospheric pressure and oxygen, rather than lower numbers of cells per leaf. To quantify this effect, the respective guard cell size per density sampling area would need to be observed. This could have led to leaves that contained fewer cells in response to higher atmospheric pressure and oxygen, supported by the lack of differences in surface stomatal index or density.

Previous work on angiosperms has demonstrated that plant cell sizes are not correlated with leaf area in developed plants (John et al., 2013). This suggests that the number of cells in a leaf determines leaf area within plants grown from seeds. While, other work suggests that changes in leaf area are likely due to the effect of outside forces acting upon developing meristem. For example, Takemura et al., (2017) demonstrated that previously developed bryophyte shoot length, epidermal cell length, leaf length, but

not leaf cell count were lowered by 10X hypergravity. This suggests that plant cells may change cellular dimensions such as length and shape in response to external forces such as higher atmospheric pressures. Changes in *H. lucidula* leaf area are not due to changes in cell number in response to external forces, but the result of changes in leaf cell shape and leaf area. This is supported by the observed smaller leaf width and leaf area by treatment. Additionally, the conditions of Takemura's study better match those of my study upon *H. lucidula*, where already developed stems reacted to changes in atmospheric conditions but did not germinate within a changed atmosphere.

The effect on leaf size due to oxygen may also be pressure related. In the *C* treatment, the partial pressure of oxygen was approximately 21.7 kPa, while the effective pressure was 24.8, 31.0, and 35.4 kPa for the *P*, *I* and *O+P* treatments, respectively. The leaf area and width changes with respect changes in the partial pressure of oxygen due to treatment suggests that a higher partial pressure of oxygen contributes to changes in *H. lucidula*'s developing leaf tissue. A potential mechanism for the effecting leaf development could be found in effecting the initiation of leaf primordia, either by lessening the activity of cell wall stability controlling expansin enzymes and/or through a chemically inhibiting reaction with auxin indoleacetic acid (Cleland, 2001). This suggests a physical mechanism which either directly effects the enzyme function by destabilizing enzyme structure, deduces the catalytic velocity, and by resisting the internal tem turgor pressure thought to expand cell walls. However, how oxygen is relevant to this mechanism is dubious. Alternatively, endogenous flavonoids are known to inhibit leaf development , particularly quercetin (Brown et al., 2001); however, these compounds have also been demonstrated to have antioxidant properties and reactivity to radical

oxygen (Morales et al., 2012). This would suggest that a chemical saturation of meristem flavonoids with oxygen, leading to decreased leaf primordia inhibition, would lead to increased formation of new leaves; however, this was not observed. These two different mechanisms of action could highlight the difference sensitivities to pressure and oxygen between fully developed and actively germinating plants.

Changes in leaf area effect plant function. Smaller leaves correlate to developmentally smaller effective leaf widths and less leaf margin complexity, and physically leads to less temperature dissipation across the boundary layer and smaller temperature gradient range along the length of the leaf (Leigh et al., 2017). Energy dissipation along the boundary layer is a function of leaf width (Campbell and Norman, 1998; Nobel, 2009). This suggests that plants with smaller leaf area have a narrower leaf temperature range and affects the rates of transpiration along the length of the leaf.

The leaf aspect ratio was found to be significantly smaller due to *O* but not has smaller as *P*. Oxygen also affects SLA but opposite to oxygen on leaf aspect ratio, higher SLA values were found in *O* treatment plants but not as high as in *P*. However, in *O*+*P* aspect ratio values were restored to *C* levels while SLA values were further decreased from *O*. This suggests that the presence of oxygen mitigates the effect of the higher partial pressure of oxygen.

The mechanisms effecting leaf aspect ratio and SLA are likely highly related, as higher pressure primarily lowered the aspect ratio but raised SLA and higher partial pressures of oxygen raised aspect ratio and lowered SLA. . These mechanisms changing the leaf aspect ratio and SLA are probably due to changes in the leaf area. However, the effect is not proportional, as with a smaller leaf area; as *P* and *O* leaves would have had

to also have lower masses in order to increase SLA and decreasing leaf width due to *O+P*, but *C* levels of aspect ratio suggest that *O+P* treated leaf cells were smaller and thus thinner but proportionally as wide.

I report that growing plants in chambers was able to affect *H. lucidula.* Plants not grown in chambers were significantly different: with larger leaf area, except *C*, 0.0430 ± 0.0186 cm^2, SD (433); larger leaf width 0.1154 ± 0.0245 cm, SD (433); and a smaller leaf aspect ratio 3.8160 ± 1.1002 (L:W), SD (433). The effect chambering on *H. lucidula* are likely combination of stable higher humidity and a slight pressurization from measured ambient levels of 100.6 kPa to 103.3 kPa. I do not expect the partial pressure of oxygen to be active in chambers, as a 4 kPa difference in pressure is within normal weather variations.

Surface Stomatal Morphology

The anomocytic stomatal arrangement I observed is consistent with previous studies on *Lycopodium* species (Sun et al., 2005); because of this consistency, I suggest a haplocheilic aperigenous ontology (Pant and Mehra, 1964). Regarding the stomatal sampling methodology I used, there is a disagreement by researchers in the optimal sampling area, ranging from whole microscope fields of view to box grids (McElwain and Chaloner, 1995; Poole and Kürschner, 1999; Woodward and Bazzaz, 1988). I selected a 100X sampling area of approximately one half of the total leaf width, as collected enamel peals often tore along the delicate midline due to *H. lucidula*'s small leaf size. Sampling was done across a diagonal in order to account for changes in stomatal distribution that could result from changes in leaf geometry. This produces consistent measures of stomata between different species, as some lycopsid species have

stomata along the midline while others are between the midrib and margin (Chu, 1974). Leaf measurements were taken from a grid instead of whole leaf as the higher magnification images gave the resolution necessary to distinguish between pavement cells, effectively allowing pavement cell counts for stomatal index values.

The difference between the pre-treatment and post-treatment stomatal density to stomatal index is minimal (Figure 4.1). The y-intercept of 0.118 for post-treatment leaves suggest more internal variation leading to a wider sampling distribution. Considering no significant effects were found regarding change in SI or D due to treatment, this is likely due to random error as this value and zero are both the within the pre-treatment and post-treatment standard error of the intercept of 0.226 and 0.338, respectively. This intercept was additionally found to have no significant ($p = 0.134$) difference to the pre-treatment line by homoscedastic t-test. Despite this analysis, these two correlations are essentially the same, as the difference between the two resulting y-intercepts is roughly 0.12% and is insubstantial in terms of stomatal index. Additionally, the slope of each line was not found to be significantly different ($p = 0.508$) by heteroscedastic z-test, having standard errors of 2360 and 3350, respectively.

Analysis of the correlation between stomatal density and index also indicates that stomatal density measures were not continuous distributed, unlike index. This pattern is caused by the method used to determine stomatal density, as guard cells were not counted partially but as either present or not present within the sampling area. This lead to several index values being observed within a single discrete stomatal density. The relationship I found between stomatal density and index can be used to approximate *H. lucidula*'s stomatal index without the counting of individual pavement cells.

Analysis of the effect of the mean aperture to maximum aperture area to modeled leaf conductance defines the operational stomatal conductance. I assume the use of a_{mean} to represents a functional gas exchange surface area, instead of a leaf with uniformly open stomatal at maximum size. I found that this allows a better fit between a_{max} models and gathered conductance values (Figure 4.2), leading to less model-overestimation compared to purely theoretical measures; this is similar to Fanourakis et al., (2015), except that I use actual aperture measurements as opposed to models. The modeled operation conductance ratio φ_{g_S} produces a calibration curve between measures of a_{mean} and a_{max} values. I propose this ratio as a relevant correction factor, due to the larger statistical robustness of mean measures of central tendency than outlier susceptible maxima. However, it is unclear whether φ_{g_S} is a global constant or is species specific.

Post-Treatment Subsurface Stomatal Morphology

The interior tissues of *H. lucidula* stomata were characterized from SEM that allowed more accurate measurements of the stomatal pore. However, some samples were affected by light refraction from resin impregnated cell walls. SEM techniques also allowed the coupling of a backscatter ion detector to the microscope; producing a deeper signal than of the primary electron beam signal, giving topological information. By using an organic resin procedure similar to that used for TEM, the resin did not produce a background signal and the topographic information of the leaf section samples was maintained. The topographic information produced by backscatter ion detection primarily elucidated between preparation artefacts and substomatal aerenchyma, in addition to allowed better identification of guard cell contractile vacuoles, mitochondria, and

chloroplast organelles. Imaging of the substomatal space of *H. lucidula* was characterized by aerenchyma surrounded by a ring of mesophyll cells.

H. lucidula's mesophyll cells were found to form unbroken rings of cells around the stomatal inner chamber in some images while in other images this ring of cells was seemingly punctured by aerenchymal intrusions. Consequently, it is suggested that the substomatal cavities of *H. lucidula* are characterized by a 'basket' motif of a single layer of mesophyll cells around the stomatal inner cavity, instead of a mass of mesophyll cells directly beneath the stomatal pore (Figure C.1). As it was observed that the stomatal inner ledge of *H. lucidula* was highly reduced and smaller than a micrometer, I reasoned that the inner cavity is continuous with the substomatal cavity.

Development of a Modified Stomatal Conductance Model

I observed that *H. lucidula*'s aerenchymal tissue was generally situated directly below the stomatal complex, while the surround mesophyll was generally palisade tissue. This suggests that the inclusion of the g_{SSC} value within my proposed g_{pore} model supersedes the need of the traditional, but rarely utilized, g_{ias} value (Nobel, 2009).

Using my modified g_{pore} model of stomatal conductance, the disparity between modeled g_{sur} values and measured IRGA g_{CO_2} values is due to partitioning of the stomatal pore into four cavities. However, modeling produces optimal values that overestimate gas flow. To counter this, I define the operational leaf conductance error ($g_{l,op}$) as the ratio (φ_g) between IRGA (g_l) and modeled ($g_{l,op}$) leaf conductance:

$$\varphi_g = \frac{g_l}{g_{l,op}}$$

$$g_l = \varphi_g \cdot g_{l,op}$$

This analysis of modeled data (Table 4.4) suggests that a similar treatment of my *H. lucidula* proposed g_{pore} model data would yield a φ_g value of 0.23, similar to the 0.2 value reported by previous work (McElwain et al., 2016a). Since these values are essentially the same, this suggests that the effect of mesophyll conductance could be described in McElwain's terms. This correction factor could indicate the presence and calculation of leaf mesophyll conductance (g_m). This further supports a model of leaf gas assimilation whereby the total photosynthetic productivity is limited by mesophyll tissue resistance (Niinemets et al., 2009). However, the comparisons in Figure 4.3 suggest that this method could be flawed. Despite my model being able to increase the fit between current models and IRGA measurements by decreasing the slope, the presence of a non-zero y-intercept and the non-linear rate of change between each line suggests that the true correction is a non-linear function. Alternatively, this could well be an artefact caused by the relatively small magnitude of *H. lucidula* IRGA measurements.

IRGA Measured Physiology

While the rate of photosynthesis did not change, it is likely that a response was hidden within the relatively lower levels of gas exchange observed (McElwain et al., 2016b). My results showed that higher atmospheric pressure lead to higher stomatal gas conductance but higher atmospheric oxygen lead to lower stomatal gas conductance. These two effects are likely additive and subtractive, since the response of *O+P* was not significantly different from that of *C* levels.

Previous research has indicated that equilibrium between the processes of photosynthesis and photorespiration in C3 plants is achieved at approximately 69 ppm CO_2 in 31% O_2 (Tolbert et al., 1995). When accounting for maintenance respiration, the

optimal atmospheric O_2:CO_2 of 1200 leads to 260 ppm carbon dioxide at 31% atmospheric oxygen (Sage and Coleman, 2001). This suggests that *O* treatment plants preferred photosynthesis to photorespiration, wherein the concentration of atmospheric carbon dioxide was approximately at atmospheric levels of 400 ppm; however considering that the O_2:CO_2 for *O* at ambient 400 ppm CO_2 is around 780 compared to the *C* treatment O_2:CO_2 of around 525. This suggests that *O* treated plants were inherently less capable to efficiently assimilate CO_2 than the control. This plant stress has been considered to be a source of higher plant diversity (Igamberdiev and Lea, 2006). However, since higher photosynthesis was not observed, this seems to suggest that the rate of *H. lucidula*'s metabolic activity was likely enhanced by the higher atmospheric oxygen and is not limited by the photosynthetic rate.

The higher change in internal CO_2 in the *O+P* treatment, but not in the *O* and *P* plants, suggests a combination of effects. In combination with my leaf morphology results, this further suggests that *H. lucidula* and possibly other lycopsids are capable of reacting to changes in pressures due to changes in the partial pressure of oxygen, but internally is also dependent upon gas fraction. Gas exchange results (Figure 4.4) show that internal CO_2 were higher within *H. lucidula* in response to higher atmospheric pressure and oxygen, yet not due to either individually. This evidence seems to suggest that pressure is able to better 'pack' oxygen into aerenchyma, intercellular air spaces known to be within both angiosperms and lycopsids.

The change in ΦPSII, ETR, and PLUE for the plants among the treatments indicates a potential change in chloroplast morphology and function (Figure 4.4 and 4.5). The force of hypergravity upon developed angiosperms has been demonstrated to

decrease leaf chlorophyll content, the same as a decrease in the superficial density of chlorophyll (Vidyasagar et al., 2014). This suggests a mechanism for the decrease in organization in *P* relative to *C* treatment. While swelling of the thylakoid lamellae (Pribil et al., 2014) could explain how higher oxygen concentrations led to lower PLUE for the *O* and *O+P* post-treatment values, while *C* and *P* treatment values were higher. This swelling has been previously implicated in being produced by the epoxidation of zeaxanthin to violaxanthin causing less photoprotectivity (Johnson et al., 2011). This seems to suggest that the increases in the partial pressure of oxygen shifted the equilibrium of xanthophyll products towards thicker constituents.

Post-Treatment Ribulose-1,5-Bisphosphate Carboxylase/Oxygenase

A key trend in RuBisCO expression is that *O+P* leaf RuBisCO levels were the highest and that the average *C* leaf RuBisCO levels were the lowest (Figure 4.6). The effect of pressure is likely what drives this mechanism of change, as *P* and *O+P* leaves required more RuBisCO protein to accomplish similar or higher levels of carbon dioxide conductance. Higher levels of carbon dioxide influx mechanistically suggest a necessarily larger source and/or sink strength; however, these RuBisCO results suggest that with larger source strength there is also a larger the sink strength.

A possible physical mechanism to interpret the effect of higher atmospheric pressures upon enzyme carbon dioxide gas assimilation has been found within recent biochemical studies, indicating that rate which proteins harmonically change shape over time is effected by salinity, in addition to temperature and pH (Makowski et al., 2008). This phenomenon could suggest that increase pressures have an inhibitory effect upon enzyme reaction rates given that proteins are sensitive to local cytosolic water potential,

whereby pressures are capable of changing enzyme activity by affecting-substrate pocket sizes. Additionally, the effect of water potentials on isotope specificities have already been previously demonstrated (Farquhar et al., 1982; Ambrose et al., 2010; Mullin et al., 2009), suggesting that the kinetic isotope effect as a possible co-mechanism, if cellular internal water potentials are capable of being effected by atmospheric pressure.

Concluding Remarks

Research into the effect of atmospheric pressures upon plants and living tissues is relatively novel (Goyette et al., 2012; Murukesan et al., 2015). Although treatment at various atmospheric conditions was not able to change the rate of *H. lucidula* photosynthesis, our results are also consistent with previous work indicating lycopsid transpiration rates are not sensitive to changes in VPD due to temperature (Soni et al., 2012). However, plants in higher atmospheric pressures had significantly higher conductance in *P* and WUEi in *O+P*. This suggests that pressure has the potential of increasing the gas conductance of plants with similar subsurface stomatal characteristics for larger scale 'hyperbaric agriculture,' especially within a space and/or fresh water limited world (Hochman et al., 2017; Win et al., 2017); by maximizing productivity with carbon dioxide gas fertilization, this could also prove to be a cost-efficient manner to maintain plants within spacecraft, given the prohibitive cost of transporting water. We also suggest that the effect of higher pressures on protein activity would reasonably lead to an increase in expression in order to compensate for decreases in activity. While the activity was not observed, this is a reasonable mechanism to suggest a decrease that the sink strength of RuBisCO, upon dissolved carbon dioxide, gas was lowered by physical but also biochemical means reacting to the partial pressure of oxygen.

CHAPTER SIX

Conclusion

Lycopsid Mesophyll is Transitional to Angiosperms

This research has substantiated that the flow of gas into lycopsid plants is limited by subsurface morphological features. Additionally, we suggest that the presence of the large substomatal cavity is functionally identical to aerenchyma and generally produces the lowest conductance rates in comparison to the other three features, despite having the largest volume. Hence, a larger surface area and respective pore volume is available for gas exchange without the metabolic price of developing new stomata.

This is key, as *H. lucidula* has not been previously demonstrated to possess the ion based stomatal control mechanisms that are present within angiosperms (Brodribb and McAdam, 2011; Evert et al., 2006), a consequence of this is that these plants are able to effectively maximize stomatal aperture sizes via only guard cell water content. Additionally, recent computer modeling implicated that water use efficiency increases are due to physically changes in response to the present of large substomatal cavities (Roth-Nebelsick, 2007); while, angiosperms have been found to significantly increase the relative size of mesophyll aerenchyma in response to drought conditions (Chartzoulakis et al., 1999). This gives evidence that the aerenchyma organization of *H. lucidula* is a product of lycopsid plant evolution to maximize water use efficiency despite being unable to close their guard cells. The mechanism of action is likely through increasing carbon dioxide flux per pore volume and increased storage.

It is not-unexpected that recent research has implicated that lycopsids have a unique metabolic system wherein carbon dioxide and oxygen gas is diurnally enriched within the mesophyll tissues aerenchyma. The insensitivity of model lycopsids bulk photosynthetic carbon fixation to various atmospheric conditions can be explained how early leaves assimilated the majority of their carbon dioxide gas through their roots, transporting root carbon dioxide gas up toward photosynthetic leaves while oxygen gas was carried down to the roots through a parichnos morphology of elongated parenchymal tissues (Green, 2010). However, this would suggest that the role of the stomata was less involved in carbon dioxide gas uptake and more importantly defined transpiration.

Complications with Defining a New Metabolic Habit

A consequence of this is that the atmosphere-soil carbon dioxide gas boundary conductance is more important than atmosphere-leaf models in understanding early vascular plant photosynthesis. This would require an in-depth understanding of the microbial diversity, the degree of symbiosis with paleo-plants, and the rates of soil nitrification at these atmospheric conditions. This is seemingly confounded by laboratory terrestrial lycopsid cultivation techniques that suggests that mycorrhizal or cyanobacterial associates may not have been necessary for nutrient supply (Benca, 2014). This ultimately makes the process of modeling LPP plant gas exchange an exercise in microbial ecology or dependent on the assumption that paleosols were already saturated with free carbon dioxide.

There are several considerations to be made, in order to accurate apply an effect of soil-carbon conductance upon carbon fixation modeling in plants. In C3 plants, carbon dioxide must diffused from gas phase to liquid phase in the mesophyll in order to reach

the carboxylation protein RuBisCO, this leads to relatively low internal carbon dioxide level and carbon-fixation tends to be limited by the availability of the intermediate ribulose 1,5-bisphosphate due light-dependent reactions. In C4 plants, internal carbon dioxide is concentrated in chlorenchyma, as carbon-fixation tends to be limited by the enzyme activity of RuBisCO due to the Calvin cycle. CAM plants also concentrate carbon dioxide gas as C4 plants do, yet their ability to concentrate carbon dioxide is limited by their ability to store maleic acid; additionally, CAM idling allows these plants to survive for long period of times by re-fixing respired carbon dioxide (Taiz and Zeiger, 2010). This seems to suggest that CAM plants generally utilized triose phosphates due to the buildup of acids when at capacity (Sharkey et al., 2007). Since LPP both spatially and maybe temporally concentrates carbon dioxide, it is likely that either a RuBisCO or triose phosphate limitation is possible; however, in *H. lucidulua* which could have issues with forming a stable seal for carbon dioxide, a more spatial RuBisCO profile is expected.

Testing for LPP

Although it has been experimentally demonstrated that *H. lucidula* is RuBisCO limited by our research group, the existence of LPP is not able to be conclusively known from the current results. In order to understand whether or not LPP is a combination of other effects working in combination with one another to produce a complex physiology or a novel described physiology, testing for LPP within extant lycopsids is recommended. Reasonably, if LPP cannot be identified within more derived extant terrestrial lycopsids, then LPP's presence within arborescent extinct lycopsids would be suspect. The presence of LPP is dependent upon a plant's ability to utilize soil carbon dioxide over atmospheric carbon dioxide.

An experiment can be devised from this fact by designing a grow chamber that is inoculated with copious soil organic carbon. An air-tight bladder could be used to separate the stem of a full grown lycopsid from the air above and below the soil. Similar to rhizome respiration studies, then nitrogen gas of similar to atmospheric pressure would be need to be plumbed to the top part of the chamber while normal laboratory air would be plumbed to the soil (Laing, 1940). This approach is complicated in setup and requires specialized equipment be assembled; yet the result would a clear one- the presence of plant death after over time. Non-LPP plants would be expected to survive for significantly shorter than non-bladdered plants. Another treatment could be run alongside the full soil-atmosphere separation in order to control for the possibility that the bladder could girdle the plants and cause a false negative for LPP, which some plants have partial bladders that surround the stem the same but do not separate the soil from the atmosphere within their installed chambers.

Another approach may be taken to test for LPP that is less equipment dependent but has a more complex result. Lycopsid plants would be placed into sealed growth chambers just as before; however, ^{13}C doped carbon would be introduced into the chamber atmosphere and/or soil. The results would require the potential health risks of radioisope imaging and imaging of the localization of ^{13}C. Non-LPP plants would be expected to have more ^{13}C localization in leaf issues over root tissues when ^{13}C would be introduced as ^{13}C doped carbon dioxide gas. This approach would also require a non-treated control and a treatment where ^{13}C was introduced only into the soil and another with both doped carbon dioxide gas and organic soil carbon.

APPENDICES

APPENDIX A

Pressure Chamber Design

IRGA measurement were taken at a constant inlet CO_2 concentrations of 371.23 ± 50.38 ppm SE(53) and laboratory CO_2 concentrations of 369.45 ± 51.75 ppm SE(54). This data is characterized by large experimental variance. This is likely due to the several hours necessary to conduct each set of measurements. Evidence of this can be found in that the air pressure varied from 101.46 ± 0.31 kPa, SD (54) and, despite cooling, the air temperature sensor read 28.70 ± 1.72 ^{o}C, SD (54). Fluorescence measurements taken at 364.49 ± 89.76 μmol m^{-2} s^{1}, SE (53) PAR.

Chambers were designed to allow chambers pressures to reach the maximum sensor limit of 120 kPa. Further inquiry focused upon the post middle-late Pennsylvanian transition model of *H. lucidula* subjected to higher pressures (118.1 kPa) and oxygen (~30 %) within hardier, yet still relatively cheap, laboratory constructed pressure chambers. These atmospheric pressures corresponded to Carboniferous levels between 400 m to 600 m above sea level at 15-22 ^{o}C (Graham et al., 1995; Poulsen et al., 2015; Campbell and Norman, 1998). Control ambient lab conditions were calibrated to slightly over sea level pressure (103.3 kPa) in order to allow a calibrated air turnover rate, similar to that of the non-pressurized preliminary study and corresponding to US Standard Atmosphere at ~22 ^{o}C (1976).

Each plant was maintained in individually plumbed chambers designed to keep a high relative humidity and provide pressurization. The concentration of outlet carbon

dioxide gas (ppm), concentration internal oxygen gas (%), inlet pressure (kPa), and internal humidity was monitored via two Vernier LabPro Systems attached to four chambers, one per treatment, drilled to fit removable proprietary sensors (Figure A.1).

Figure A.1 – A model of a laboratory constructed chamber, detailing a top intake and regulated exhaust value. Oxygen, carbon dioxide, and pressure sensing was measured via dedicated chambers, piped in parallel and featuring holes for sensors.

APPENDIX B

Representative Atmospheric Conditions

In my work to describe the physical characteristics of Paleozoic atmospheres, I was unable to reproduce the work of Graham et al. 1995's paper. Working backwards from these representative 285 Mya and 250 Mya atmospheres of 100 kPa at 0 ^{o}C STP US Standard Atmosphere gas compositions, a less precise NIST 1988 8.314471 gas constant magnitude, and 0 ^{o}C at 273.16 K did not produce feasible calculated atmospheres (Graham et al., 1995; Moldover et al., 1988)- respectively, producing a 1.56 kg m^{-3} atmosphere weighing 35.42912 g mol^{-1} dry with molar volume of 0.018920 m^3 mol^{-1} and consisting of 35.3% O2, 80.690% N2, 300 ppm CO2, and 0.797 % Ar and a 1.12 kg m^{-3} atmosphere weighing 25.436 g mol^{-1} dry with molar volume of 0.025681 m^3 mol^{-1} consisting of 35.3 % O2, 57.877 % N2, 900 ppm CO2, and 0.572 % Ar. Instead, by assuming that the partial pressure of atmospheric nitrogen and argon gas remained constant as per Graham's calculations, I suggest that these would respectively yield atmospheres at 114.348 kPa weighing 29.337 g mol^{-1} dry with molar volume of 0.019862 m^3 mol^{-1} at 1.477 kg m^{-3} and 94.208 kPa weighing 28.7753 g mol^{-1} dry with molar volume of 0.024108 m^3 mol^{-1} at 1.194 kg m^{-3}. I determined the physical characteristics of my experimental atmospheric conditions as a 0.9878:0.0114 N_2:Ar split, accounting for 404.02 ppm CO_2 (Table B.1).

Table B.1 - The physical characteristics of examined and the produced chamber atmospheres based on International Standard Atmosphere, U. S. Standard Atmosphere, and ISO2533:1975 pressure conditions of 101.325 kPa (in bold) at 15 ^{o}C MSL (in italics), and considering the constituent gas changes associated with different concentrations of atmospheric oxygen (in italics). Heat capacity at a constant pressure was calculated using $MW_{dry\ air}$ 7/2R at 0^{o}C; density was calculated assuming ideal gas conditions. Additionally in bold are Graham's estimated atmospheres at a standard temperature of 0 ^{o}C and produced chamber atmospheres at 22 ^{o}C. Preliminary CO_2 values are from June 2014, while standard CO_2 values are updated to February 2016 (asterisked) (Tans and Keeling, 2016). The preliminary atmosphere here indicates the approximate atmosphere produced for initial work detailing lycopsid plant response to chambering (unpublished data).

Measure		Graham 250 Mya	Graham 285 Mya	STD*	*C*	Prelim.	*P*	*O*	*O+P*
[O_2] (%)		*15.1000*	*35.3000*	*20.9476*	*20.9476*	*20.9476*	*20.9476*	*30.0000*	*30.0000*
[N_2] (%)		83.860	63.907	78.084	78.084	78.084	78.084	69.144	69.144
[Ar] (%)		1.003	0.764	0.934	0.934	0.934	0.934	0.799	0.799
[CO_2] (ppm)		900.00	300.00	404.02*	404.02	401.15	404.02	404.02	404.02
$MW_{dry\ air}$ (g mol^{-1})		28.763	29.516	28.967	28.967	28.967	28.967	29.305	29.305
C_P (J g^{-1} K^{-1})		1.0117	0.9859	1.0046	1.0046	1.0046	1.0046	0.9930	0.9930
MW_{wv}/MW_{air}		0.626	0.610	0.622	0.622	0.622	0.622	0.615	0.615
P_a (kPa)	-10^{o}C	86.161	113.061	92.534	92.100	93.616	105.296	92.100	105.296
	-5^{o}C	87.798	115.209	94.292	93.850	95.395	107.296	93.850	107.296
	0^{o}C	**89.435**	**117.357**	96.050	95.600	97.173	109.297	95.600	109.297
	5^{o}C	91.072	119.505	97.809	97.350	98.952	111.298	97.350	111.298
	10^{o}C	92.709	121.654	99.567	99.100	100.731	113.298	99.100	113.298
	15^{o}C	*94.346*	*123.802*	***101.325***	*100.850*	*102.510*	*115.299*	*100.850*	*115.299*
	20^{o}C	95.983	125.950	103.083	102.600	104.288	117.300	102.600	117.300
	22^{o}C	96.638	126.809	103.786	**103.300**	**105.000**	**118.100**	**103.300**	**118.100**
	25^{o}C	97.620	128.098	104.841	104.350	106.067	119.300	104.350	119.300
	30^{o}C	99.257	130.247	106.600	106.100	107.846	121.301	106.100	121.301
	35^{o}C	100.895	132.395	108.358	107.850	109.625	123.302	107.850	123.302
	40^{o}C	102.532	134.543	110.116	109.600	111.404	125.302	109.600	125.302
ρ_{air} (kg m^{-3})	-10^{o}C	1.240	1.670	1.341	1.368	1.390	1.564	1.384	1.582
	-5^{o}C	1.217	1.639	1.316	1.342	1.364	1.534	1.358	1.552
	0^{o}C	**1.195**	**1.609**	1.292	1.318	1.339	1.506	1.333	1.524
	5^{o}C	1.173	1.580	1.269	1.294	1.315	1.479	1.309	1.497
	10^{o}C	1.153	1.552	1.247	1.271	1.292	1.453	1.286	1.470
	15^{o}C	*1.133*	*1.525*	***1.225***	*1.249*	*1.270*	*1.428*	*1.264*	*1.445*
	20^{o}C	1.113	1.499	1.204	1.228	1.248	1.404	1.242	1.420
	22^{o}C	1.106	1.489	1.196	**1.219**	**1.239**	**1.394**	**1.234**	**1.410**
	25^{o}C	1.095	1.474	1.184	1.207	1.227	1.380	1.221	1.396
	30^{o}C	1.077	1.450	1.164	1.187	1.207	1.357	1.201	1.373
	35^{o}C	1.059	1.426	1.146	1.168	1.187	1.335	1.182	1.351
	40^{o}C	1.042	1.403	1.127	1.149	1.168	1.314	1.163	1.329

Table B.1 – continued

Measure		Graham 250 Mya	Graham 285 Mya	STD*	*C*	Prelim.	*P*	*O*	*O+P*
[O_2] (%)		*15.1000*	*35.3000*	*20.9476*	*20.9476*	*20.9476*	*20.9476*	*30.0000*	*30.0000*
[N_2] (%)		83.860	63.907	78.084	78.084	78.084	78.084	69.144	69.144
[Ar] (%)		1.003	30.444	0.934	0.934	0.934	0.934	0.799	0.799
[CO_2] (ppm)		900.00	300.00	404.02*	404.02	401.15	404.02	404.02	404.02
$MW_{dry\ air}$ (g mol^{-1})		28.763	29.516	28.967	28.967	28.967	28.967	29.305	29.305
C_P (J g^{-1} K^{-1})		1.0117	0.9859	1.0046	1.0046	1.0046	1.0046	0.9930	0.9930
MW_{wv}/MW_{air}		0.626	0.610	0.622	0.622	0.622	0.622	0.615	0.615
M_V (m^3 mol^{-1})	-10°C	0.023191	0.017673	0.021593	0.021181	0.020838	0.018526	0.021181	0.018526
	-5°C	0.023631	0.018009	0.022004	0.021583	0.021234	0.018878	0.021583	0.018878
	0°C	**0.024072**	**0.018345**	0.022414	0.021985	0.021629	0.019230	0.021985	0.019230
	5°C	0.024513	0.018680	0.022824	0.022388	0.022025	0.019582	0.022388	0.019582
	10°C	0.024953	0.019016	0.023235	0.022790	0.022421	0.019934	0.022790	0.019934
	15°C	*0.025394*	*0.019352*	***0.023645***	*0.023193*	*0.022817*	*0.020286*	*0.023193*	*0.020286*
	20°C	0.025835	0.019688	0.024055	0.023595	0.023213	0.020638	0.023595	0.020638
	22°C	0.026011	0.019822	0.024219	**0.023756**	**0.023372**	**0.020779**	**0.023756**	**0.020779**
	25°C	0.026275	0.020024	0.024465	0.023998	0.023609	0.020990	0.023998	0.020990
	30°C	0.026716	0.020359	0.024876	0.024400	0.024005	0.021342	0.024400	0.021342
	35°C	0.027156	0.020695	0.025286	0.024803	0.024401	0.021694	0.024803	0.021694
	40°C	0.027597	0.021031	0.025696	0.025205	0.024797	0.022046	0.025205	0.022046

APPENDIX C

Semi-thin Sectioning of SSC

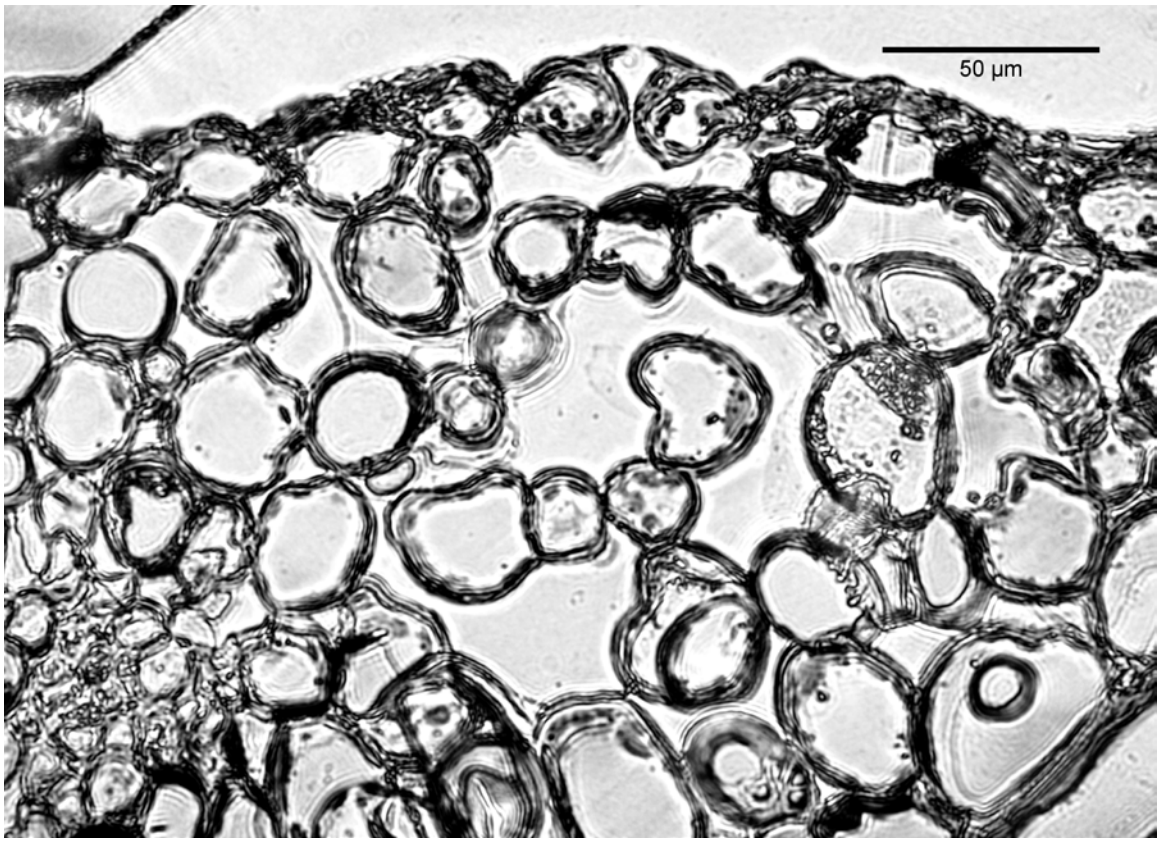

Figure C.1 –Contrast adjusted, light transmission micrograph at 400X of *O+P* 400 nm semi-thin lateral new leaf section within EMBED 812 resin. Seemingly unchanged from *C*, this clearly displays the stomatal cavities, “basket” substomatal cavity motif, mesophyll aerenchyma, and vascular bundle.

APPENDIX D

IRGA Figure Data

Table D.1 – The mean ± one standard error *(sample size)* IRGA gas exchange and fluorescence and combined physiological parameters of pre-treatment and post-treatment new growth of *H. lucidula*, detailing: stomatal carbon dioxide gas conductance, internal CO_2, photosystem II quantum yield, linear electron transport rate, PAR light use efficiency, instantaneous water use efficiency, and intrinsic water use efficiency (Figure 4.4 and 4.5). Notation letters indicate values which were found to change significantly ($p \leq 0.05$), and notation numbers indicate the number of plants trimmed from each sample due to data analysis.

Treatment	Measure	Pre-treatment	Post-treatment	Note
C (6)	Pn (µmol m^{-2} s^{-1})	1.36 ± 0.73	1.50 ± 0.52	n.s.
	$g^s_{CO_2}$(mmol m^{-2} s^{-1})	9.91 ± 3.24	25.50 ± 19.34	a,b;1
	C_i (ppm)	321.22 ± 38.72	262.25 ± 29.83	a
	ΦPSII	0.69 ± 0.11	0.54 ± 0.16	a
	ETR (µmol m^{-2} s^{-1})	97.66 ± 27.72	55.57 ± 8.53	a
	PLUE (g_c MJ^{-1})	0.2290 ± 0.1266	0.3581 ± 0.1640	a,b;1
	WUE	0.9676 ± 0.0820	1.5200 ± 0.7485	n.s
	WUEi	0.1142 ± 0.0412	0.0649 ± 0.0252	a
P (8)	Pn (µmol m^{-2} s^{-1})	0.79 ± 0.71	1.19 ± 0.48	n.s.
	$g^s_{CO_2}$(mmol m^{-2} s^{-1})	8.11 ± 7.14	31.67 ± 34.84	c;1
	C_i (ppm)	310.16 ± 26.25	244.65 ± 28.61	a
	ΦPSII	0.69 0.07	0.27 ± 0.08	b
	ETR (µmol m^{-2} s^{-1})	129.42 ± 26.03	39.62 ± 6.07	b
	PLUE (g_c MJ^{-1})	0.1099 ± 0.11532	0.2010 ± 0.0939	a
	WUE	0.8350 ± 0.3429	1.0747 ± 0.5630	
	WUEi	0.0989 ± 0.0271	0.0674 ± 0.0354	a;1

Table D.1 – continued

Treatment	Measure	Pre-treatment	Post-treatment	Note
O (6)	Pn (µmol m^{-2} s^{-1})	1.69 ± 0.98	0.87 ± 0.48	n.s.
	$g^{s}_{CO_2}$(mmol m^{-2} s^{-1})	27.71 ± 39.63	14.30 ± 8.83	a,c
	C_i (ppm)	297.20 ± 53.86	248.68 ± 26.31	a
	ΦPSII	0.61 ± 0.11	0.28 ± 0.16	a,b
	ETR (µmol m^{-2} s^{-1})	106.68 ± 23.01	34.76 ± 7.19	a,b
	PLUE (g_c MJ^{-1})	0.2330 ± 0.1485	0.1703 ± 0.1117	b
	WUE	1.4167 ± 0.3832	1.0899 ± 0.5974	
	WUEi	0.1096 ± 0.0475	0.0632 ± 0.0154	a
O+P (8)	Pn (µmol m^{-2} s^{-1})	3.06 ± 0.22	1.29 ± 0.58	n.s;3
	$g^{s}_{CO_2}$(mmol m^{-2} s^{-1})	161.89 ± 223.41	117.49 ± 168.80	b;2
	C_i (ppm)	163.68 ± 20.84	266.10 ± 52.11	b
	ΦPSII	0.67 ± 0.09	0.40 ± 0.19	a,b;1
	ETR (µmol m^{-2} s^{-1})	116.48 ± 13.78	54.78 ± 7.67	a,b
	PLUE (g_c MJ^{-1})	0.4120 ± 0.0555	0.1912 ± 0.0476	b;3
	WUE	0.6779 ± 0.4377	0.9932 ± 0.1722	
	WUEi	0.0310 ± 0.0311 [b]	0.0504 ± 0.0369 [b]	4

REFERENCES CITED

Aliniaeifard, S., Malcolm Matamoros, P., and van Meeteren, U. (2014). Stomatal malfunctioning under low Vapor Pressure Deficit (VPD) conditions: Induced by alterations in stomatal morphology and leaf anatomy or in the ABA signaling? Physiol. Plant.

Ambrose, A.R., Sillett, S.C., Koch, G.W., Van Pelt, R., Antoine, M.E., and Dawson, T.E. (2010). Effects of height on treetop transpiration and stomatal conductance in coast redwood (Sequoia sempervirens). Tree Physiol. *30*, 1260–1272.

Anfodillo, T., Di Bisceglie, D.P., and Urso, T. (2002). Minimum cuticular conductance and cuticle features of Picea abies and Pinus cembra needles along an altitudinal gradient in the Dolomites (NE Italian Alps). Tree Physiol. *22*, 479–487.

Armond, P.A., Schreiber, U., and Björkman, O. (1978). Photosynthetic acclimation to temperature in the desert shrub, Larrea divaricata II. Light-harvesting efficiency and electron transport. Plant Physiol. *61*, 411–415.

Arrigo, N., Therrien, J., Anderson, C.L., Windham, M.D., Haufler, C.H., and Barker, M.S. (2013). A total evidence approach to understanding phylogenetic relationships and ecological diversity in Selaginella subg. Tetragonostachys. Am. J. Bot. *100*, 1672–1682.

Bateman, R.M. (1990). The Relationship between Formal and Informal Nomenclature and Phylogeny in Higher Taxa: A Pedant's Perspective on the Lycopsids. Taxon *39*, 624.

Beck, C.B. (1962). Reconstructions of Archaeopteris, and Further Consideration of its Phylogenetic Position. Am. J. Bot. *49*, 373.

Beerling, D. (1998). Short communication. Stomatal responses of the "living fossil" Ginkgo biloba L. to changes in atmospheric CO2 concentrations. J. Exp. Bot. *49*, 1603–1607.

Beerling, D.J., Osborne, C.P., and Chaloner, W.G. (2001). Evolution of leaf-form in land plants linked to atmospheric CO2 decline in the Late Palaeozoic era. Nature *410*, 352–354.

Benca, J.P. (2014). Cultivation Techniques for Terrestrial Clubmosses (Lycopodiaceae): Conservation, Research, and Horticultural Opportunities for an Early-Diverging Plant Lineage. Am. Fern J. *104*, 25–48.

Berner, R.A. (2009). Phanerozoic atmospheric oxygen: New results using the GEOCARBSULF model. Am. J. Sci. *309*, 603–606.

Bertrand, C.-E. (1891). Remarques sur le Lepidodendron harcourtii de Witham (Au Siège des Facultés).

Bierhorst, D.W. (1971). Morphology of Vascular Plants (NY: The Macmillan Company).

Bischof, J.C., Wolkers, W.F., Tsvetkova, N.M., Oliver, A.E., and Crowe, J.H. (2002). Lipid and protein changes due to freezing in Dunning AT-1 cells. Cryobiology *45*, 22–32.

Bolz, R.E., and Tuve, G.L. (1973). CRC handbook of tables for applied engineering science (Cleveland, Ohio: CRC Press).

Brodribb, T.J., and McAdam, S.A.M. (2011). Passive Origins of Stomatal Control in Vascular Plants. Science *331*, 582–585.

Brown, D.E., Rashotte, A.M., Murphy, A.S., Normanly, J., Tague, B.W., Peer, W.A., Taiz, L., and Muday, G.K. (2001). Flavonoids Act as Negative Regulators of Auxin Transport in Vivo in Arabidopsis. Plant Physiol. *126*, 524–535.

Came, R.E., Eiler, J.M., Veizer, J., Azmy, K., Brand, U., and Weidman, C.R. (2007). Coupling of surface temperatures and atmospheric CO2 concentrations during the Palaeozoic era. Nature *449*, 198–201.

Campbell, G.S., and Norman, J.M. (1998). Introduction to Environmental Biophysics (New York: Springer).

Cao, E., Chen, Y., Cui, Z., and Foster, P.R. (2003). Effect of freezing and thawing rates on denaturation of proteins in aqueous solutions. Biotechnol. Bioeng. *82*, 684–690.

Chartzoulakis, K., Patakas, A., and Bosabalidis, A. (1999). Comparative Study on Gas Exchange, Water Relations and Leaf Anatomy of Two Olive Cultivars Grown under Well-Irrigated and Drought Conditions. Z. Für Naturforschung C *54*.

Chu, M.C.-Y. (1974). A Comparative Study of the Foliar Anatomy of Lycopodium Species. Am. J. Bot. *61*, 681.

Cleland, R.E. (2001). Unlocking the mysteries of leaf primordia formation. Proc. Natl. Acad. Sci. *98*, 10981–10982.

Constable, J.V.H., Grace, J.B., and Longstreth, D.J. (1992). High Carbon Dioxide Concentrations in Aerenchyma of Typha latifolia. Am. J. Bot. *79*, 415.

Crane, P.R., Herendeen, P., and Friis, E.M. (2004). Fossils and plant phylogeny. Am. J. Bot. *91*, 1683–1699.

Cuhadar, S., Koseoglu, M., Atay, A., and Dirican, A. (2013). The effect of storage time and freeze-thaw cycles on the stability of serum samples. Biochem. Medica 70–77.

Dacey, J.W.H. (1980). Internal Winds in Water Lilies: An Adaptation for Life in Anaerobic Sediments. Science *210*, 1017–1019.

DiMichele, W.A., and Bateman, R.M. (1996). The Rhizomorphic Lycopsids: A Case-Study in Paleobotanical Classification. Syst. Bot. *21*, 535.

Dimichele, W.A., and Phillips, T.L. (1985). Arborescent lycopod reproduction and paleoecology in a coal-swamp environment of late Middle Pennsylvanian age (herrin coal, Illinois, U.S.A.). Rev. Palaeobot. Palynol. *44*, 1–26.

Dimichele, W.A., and Phillips, T.L. (1988). Paleoecology of the Middle Pennsylvanian-age Herrin Coal Swamp (Illinois) near a contemporaneous river system, the Walshville paleochannel. Rev. Palaeobot. Palynol. *56*, 151–176.

Dimichele, W.A., Montañez, I.P., Poulsen, C.J., and Tabor, N.J. (2009). Climate and vegetational regime shifts in the late Paleozoic ice age earth. Geobiology *7*, 200–226.

Dow, G.J., Bergmann, D.C., and Berry, J.A. (2014). An integrated model of stomatal development and leaf physiology. New Phytol. *201*, 1218–1226.

Drew, M.C., He, C.-J., and Morgan, P.W. (2000). Programmed cell death and aerenchyma formation in roots. Trends Plant Sci. *5*, 123–127.

Evert, R.F., Esau, K., and Esau, K. (2006). Esau's Plant anatomy: meristems, cells, and tissues of the plant body: their structure, function, and development (Hoboken, N.J: Wiley-Interscience).

Fanourakis, D., Giday, H., Milla, R., Pieruschka, R., Kjaer, K.H., Bolger, M., Vasilevski, A., Nunes-Nesi, A., Fiorani, F., and Ottosen, C.-O. (2015). Pore size regulates operating stomatal conductance, while stomatal densities drive the partitioning of conductance between leaf sides. Ann. Bot. *115*, 555–565.

Farquhar, G.D., von Caemmerer, S. von, and Berry, J.A. (1980). A biochemical model of photosynthetic CO2 assimilation in leaves of C3 species. Planta *149*, 78–90.

Farquhar, G.D., O'leary, M.H., and Berry, J.A. (1982). On the relationship between carbon isotope discrimination and the intercellular carbon dioxide concentration in leaves. Funct. Plant Biol. *9*, 121–137.

Flexas, J., Escalona, J.M., and Medrano, H. (1998). Down-regulation of photosynthesis by drought under field conditions in grapevine leaves. Aust. J. Plant Physiol. *25*, 893.

Franks, P.J., and Farquhar, G.D. (2001). The effect of exogenous abscisic acid on stomatal development, stomatal mechanics, and leaf gas exchange in Tradescantia virginiana. Plant Physiol. *125*, 935–942.

Friedman, W.E., and Cook, M.E. (2000). The origin and early evolution of tracheids in vascular plants: integration of palaeobotanical and neobotanical data. Philos. Trans. R. Soc. B Biol. Sci. *355*, 857–868.

Goyette, B., Vigneault, C., Charles, M.T., and Raghavan, V.G.S. (2012). Effect of hyperbaric treatments on the quality attributes of tomato. Can. J. Plant Sci. *92*, 541–551.

Graham, J.B., Dudley, R., Aguilar, N.M., and Gans, C. (1995). Implications of the late Paleozoic oxygen pulse for physiology and evolution.

Green, W. a. (2014). The Parichnos Problem and the Function of Aerenchyma in the Lycopsida. Bull. Peabody Mus. Nat. Hist. *55*, 191–200.

Green, W.A. (2010). The function of the aerenchyma in arborescent lycopsids: evidence of an unfamiliar metabolic strategy. Proc. R. Soc. B Biol. Sci. *277*, 2257–2267.

Gueidan, C., Ruibal, C., de Hoog, G.S., and Schneider, H. (2011). Rock-inhabiting fungi originated during periods of dry climate in the late Devonian and middle Triassic. Fungal Biol. *115*, 987–996.

Haworth, M., Elliott-Kingston, C., and McElwain, J.C. (2011). Stomatal control as a driver of plant evolution. J. Exp. Bot. *62*, 2419–2423.

Heinsoo, K. (1999). Cuticular and Stomatal Antechamber Conductance to Water Vapour Diffusions in Picea Abies (L.) Karst. Tartu.

Hill, T.G. (1906). On the presence of a parichnos in recent plants. Ann. Bot. 267–273.

Hochman, Z., Gobbett, D.L., and Horan, H. (2017). Climate trends account for stalled wheat yields in Australia since 1990. Glob. Change Biol. n/a-n/a.

Igamberdiev, A.U., and Lea, P.J. (2006). Land plants equilibrate O2 and CO2 concentrations in the atmosphere. Photosynth. Res. *87*, 177–194.

John, G.P., Scoffoni, C., and Sack, L. (2013). Allometry of cells and tissues within leaves. Am. J. Bot. *100*, 1936–1948.

Johnson, M.P., Brain, A.P., and Ruban, A.V. (2011). Changes in thylakoid membrane thickness associated with the reorganization of photosystem II light harvesting complexes during photoprotective energy dissipation. Plant Signal. Behav. *6*, 1386–1390.

Kenrick, P., and Crane, P.R. (1997). The origin and early evolution of plants on land. Nature *389*, 33–39.

Konrad, W., Roth-Nebelsick, A., and Grein, M. (2008). Modelling of stomatal density response to atmospheric. J. Theor. Biol. *253*, 638–658.

Laing, H.E. (1940). Respiration of the Rhizomes of Nuphar Advenum and Other Water Plants. Am. J. Bot. *27*, 574.

Lang, W.H., and Cookson, I.C. (1935). On a flora, including vascular land plants, associated with Monograptus, in rocks of Silurian age, from Victoria, Australia. Philos. Trans. R. Soc. Lond. B. Biol. Sci. *224*, 421–449.

Leigh, A., Sevanto, S., Close, J. d., and Nicotra, A. b. (2017). The influence of leaf size and shape on leaf thermal dynamics: does theory hold up under natural conditions? Plant Cell Environ. *40*, 237–248.

Li, C., and Edwards, D. (1997). A new microphyllous plant from the Lower Devonian of Yunnan Province, China. Am. J. Bot. *84*, 1441–1441.

Li, C.-S., Hueber, F.M., and Hotton, C.L. (2000). A neotype for Drepanophycus spinaeformis Göppert 1852. Can. J. Bot. *78*, 889–902.

Löve, A., and Löve, D. (1958). Cytotaxonomy and Classification of Lycopods. The Nucleus *1*, 1–10.

Ma, Z., Cooper, C., Kim, H.-J., and Janick-Buckner, D. (2009). A Study of Rubisco through Western Blotting and Tissue Printing Techniques. Cell Biol. Educ. *8*, 140–146.

Makowski, L., Rodi, D.J., Mandava, S., Minh, D.D.L., Gore, D.B., and Fischetti, R.F. (2008). Molecular Crowding Inhibits Intramolecular Breathing Motions in Proteins. J. Mol. Biol. *375*, 529–546.

Maxwell, K., and Johnson, G.N. (2000). Chlorophyll fluorescence—a practical guide. J. Exp. Bot. *51*, 659–668.

McElwain, J.C., and Chaloner, W.G. (1995). Stomatal Density and Index of Fossil Plants Track Atmospheric Carbon Dioxide in the Palaeozoic. Ann. Bot. *76*, 389–395.

McElwain, J.C., Yiotis, C., and Lawson, T. (2016a). Using modern plant trait relationships between observed and theoretical maximum stomatal conductance and vein density to examine patterns of plant macroevolution. New Phytol. *209*, 94–103.

McElwain, J.C., Montañez, I., White, J.D., Wilson, J.P., and Yiotis, C. (2016b). Was atmospheric CO2 capped at 1000 ppm over the past 300 million years? Palaeogeogr. Palaeoclimatol. Palaeoecol. *441, Part 4*, 653–658.

Medlyn, B.E. (1998). Physiological basis of the light use efficiency model. Tree Physiol. *18*, 167–176.

Medrano, H., Tomás, M., Martorell, S., Flexas, J., Hernández, E., Rosselló, J., Pou, A., Escalona, J.-M., and Bota, J. (2015). From leaf to whole-plant water use efficiency (WUE) in complex canopies: Limitations of leaf WUE as a selection target. Crop J. *3*, 220–228.

Metcalfe, C.R., and Wilkerson, H.P. (1979). The Plant Surface (Mainly Leaf). In Anatomy of the Dicotyledons, (Oxford: Clarendon Press), p.

Meyer-Berthaud, B., and Decombeix, A.-L. (2007). Palaeobotany: A tree without leaves. Nature *446*, 861–862.

Mohr, P.J., Taylor, B.N., and Newell, D.B. (2012). CODATA recommended values of the fundamental physical constants: 2010. Rev. Mod. Phys. *84*, 1527–1605.

Moldover, M.R., Trusler, J.P.M., Edwards, T.J., Mehl, J.B., and Davis, R.S. (1988). Measurement of the Universal Gas Constant R Using a Spherical Acoustic Resonator. Phys. Rev. Lett. *60*, 249–252.

Morales, J., Günther, G., Zanocco, A.L., and Lemp, E. (2012). Singlet Oxygen Reactions with Flavonoids. A Theoretical – Experimental Study. PLOS ONE *7*, e40548.

Mullin, L.P., Sillett, S.C., Koch, G.W., Tu, K.P., and Antoine, M.E. (2009). Physiological consequences of height-related morphological variation in Sequoia sempervirens foliage. Tree Physiol. *29*, 999–1010.

Murukesan, G., Leino, H., Mäenpää, P., Ståhle, K., Raksajit, W., Lehto, H.J., Allahverdiyeva-Rinne, Y., and Lehto, K. (2015). Pressurized Martian-Like Pure CO2 Atmosphere Supports Strong Growth of Cyanobacteria, and Causes Significant Changes in their Metabolism. Orig. Life Evol. Biospheres.

Niinemets, U., Diaz-Espejo, A., Flexas, J., Galmes, J., and Warren, C.R. (2009). Role of mesophyll diffusion conductance in constraining potential photosynthetic productivity in the field. J. Exp. Bot. *60*, 2249–2270.

Nobel, P.S. (2009). Physicochemical and environmental plant physiology (Amsterdam: Elsevier/Academic Press).

Pant, D.D., and Mehra, B. (1964). Developement of Stomata in Some Fern Allies. Proc. Natl. Acad. Sci. India *30, B*, 92–98.

Poole, O., and Kürschner, W.M. (1999). Stomatal density and index: the practice. In Fossil Plants and Spores: Modern Techniques, T. Jones, and N.P. Rowe, eds. (London: The Geologic Society), p.

Poulsen, C.J., Tabor, C., and White, J.D. (2015). Long-term climate forcing by atmospheric oxygen concentrations. Science *348*, 1238–1241.

Pribil, M., Labs, M., and Leister, D. (2014). Structure and dynamics of thylakoids in land plants. J. Exp. Bot. *65*, 1955–1972.

Raymond, A., Lambert, L., Costanza, S., Slone, E.J., and Cutlip, P.C. (2010). Cordaiteans in paleotropical wetlands: An ecological re-evaluation. Int. J. Coal Geol. *83*, 248–265.

Reutter, U. (1987). Growth Patterns of Gemmlings of Lycopodium lucidulum. Am. Fern J. *77*, 50.

Rickards, R.B. (2000). The age of the earliest club mosses: the Silurian Baragwanathia flora in Victoria, Australia. Geol. Mag. *137*, 207–209.

Rook, E.J.S. (2004). Huperzia lucidula, Shining Clubmoss.

Roth-Nebelsick, A. (2007). Computer-based Studies of Diffusion through Stomata of Different Architecture. Ann. Bot. *100*, 23–32.

Rouhani, I., Vines, H.M., Black, C.C., and Jr (1973). Isolation of Mesophyll Cells from Sedum telephium Leaves. Plant Physiol. *51*, 97.

Royer, D.L., Berner, R.A., Montañez, I.P., Tabor, N.J., and Beerling, D.J. (2004). CO2 as a primary driver of Phanerozoic climate. GSA Today *14*, 4.

Sage, R.F., and Coleman, J.R. (2001). Effects of low atmospheric CO2 on plants: more than a thing of the past. Trends Plant Sci. *6*, 18–24.

Schneider, C.A., Rasband, W.S., and Eliceiri, K.W. (2012). NIH Image to ImageJ: 25 years of image analysis. Nat. Methods *9*, 671–675.

Scott, A.C., Mattey, D.P., and Howard, R. (1996). New data on the formation of Carboniferous coal balls. Rev. Palaeobot. Palynol. *93*, 317–331.

Sharkey, T.D., Bernacchi, C.J., Farquhar, G.D., and Singsaas, E.L. (2007). Fitting photosynthetic carbon dioxide response curves for C(3) leaves. Plant Cell Environ. *30*, 1035–1040.

Soni, D.K., Ranjan, S., Singh, R., Khare, P.B., Pathre, U.V., and Shirke, P.A. (2012). Photosynthetic characteristics and the response of stomata to environmental determinants and ABA in Selaginella bryopteris, a resurrection spike moss species. Plant Sci. *191–192*, 43–52.

Sun, T.-X., Edwards, D., and Li, C.-S. (2005). The stomatal apparatus of Lycopodium japonicum and its bearing on the stomata of the Devonian lycophyte Drepanophycus spinaeformis. Bot. J. Linn. Soc. *149*, 209–216.

Taiz, L., and Zeiger, E. (2010). Plant physiology (Sunderland, MA: Sinauer Associates).

Takemura, K., Kamachi, H., Kume, A., Fujita, T., Karahara, I., and Hanba, Y.T. (2017). A hypergravity environment increases chloroplast size, photosynthesis, and plant growth in the moss Physcomitrella patens. J. Plant Res. *130*, 181–192.

Tans, P., and Keeling, D. (2016). Trends in Atmospheric Carbon Dioxide: Mauna Loa.

Tolbert, N.E., Benker, C., and Beck, E. (1995). The oxygen and carbon dioxide compensation points of C3 plants: possible role in regulating atmospheric oxygen. Proc. Natl. Acad. Sci. U. S. A. *92*, 11230–11233.

USDA, N. (2015). The PLANTS Database.

Vaughan, N.E., and Lenton, T.M. (2012). Interactions between reducing CO2 emissions, CO2 removal and solar radiation management. Philos. Transact. A Math. Phys. Eng. Sci. *370*, 4343–4364.

Vidyasagar, P.B., Jagtap, S.S., Dixit, J.P., Kamble, S.M., and Dhepe, A.P. (2014). Effects of Short-term Hypergravity Exposure on Germination, Growth and Photosynthesis of Triticum aestivum L. Microgravity Sci. Technol. *26*, 375–384.

Voet, D. (2013). Fundamentals of biochemistry: life at the molecular level (Hoboken, NJ: Wiley).

Wang, Q., Hao, S.-G., Wang, D.-M., and Dilcher, D.L. (2002). An anatomically preserved arborescent lycopsid, Sublepidodendron songziense (Sublepidodendraceae), from the Late Devonian of Hubei, China. Am. J. Bot. *89*, 1468–1477.

Wikström, N., and Kenrick, P. (2001). Evolution of Lycopodiaceae (Lycopsida): estimating divergence times from rbcL gene sequences by use of nonparametric rate smoothing. Mol. Phylogenet. Evol. *19*, 177–186.

Willis, K.J., and McElwain, J.C. (2002). The evolution of plants (New York: Oxford University Press).

Win, K.T., Oo, A.Z., and Bellingrath-Kimura, S.D. (2017). Influence of soil types and osmotic pressure on growth and 137Cs accumulation in blackgram (Vigna mungo L.). J. Environ. Radioact. *169–170*, 98–103.

Wolkers, W.F., Balasubramanian, S.K., Ongstad, E.L., Zec, H.C., and Bischof, J.C. (2007). Effects of freezing on membranes and proteins in LNCaP prostate tumor cells. Biochim. Biophys. Acta BBA - Biomembr. *1768*, 728–736.

Woodward, F.I., and Bazzaz, F.A. (1988). The Responses of Stomatal Density to CO 2 Partial Pressure. J. Exp. Bot. *39*, 1771–1781.

Yatsentyuk, S.P., Valiejo-Roman, K.M., Samigullin, T.H., Wilkström, N., and Troitsky, A.V. (2001). Evolution of Lycopodiaceae inferred from spacer sequencing of chloroplast rRNA genes. Russ. J. Genet. *37*, 1068–1073.

COESA. (1976). U.S. Standard Atmosphere. U.S. Government Printing Office, Washington, D.C.

(2001). Climate change 2001: the scientific basis: contribution of Working Group I to the third assessment report of the Intergovernmental Panel on Climate Change (Cambridge ; New York: Cambridge University Press).

(2006). Phosphate-buffered saline (PBS). Cold Spring Harb. Protoc. *2006*, pdb.rec8247.